



# Stress rotation — The impact and interaction of rock stiffness and faults

Karsten Reiter

TU Darmstadt, 64287 Darmstadt, Schnittspahnstraße 9

**Correspondence:** Karsten Reiter (reiter@geo.tu-darmstadt.de)

**Abstract.** It has been assumed, that the maximum compressive horizontal stress ( $S_{Hmax}$ ) orientation in the upper crust is governed on a regional scale by the same forces that drive plate motion. However, several regions are identified, where stress orientation deviates from the expected orientation due to plate boundary forces (first order stress sources), or the plate wide pattern. In some of this regions a gradual rotation of the  $S_{Hmax}$  orientation has been observed.

5 Several second and third order stress sources have been identified, which may explain stress rotation in the upper crust. For example lateral heterogeneities in the crust, such as density, petrophysical or petrothermal properties and discontinuities, like faults are identified as potential candidates to cause lateral stress rotations. To investigate several of the candidates, generic geomechanical numerical models are utilized. These models consist of up to five different units, oriented by an angle of  $60^\circ$  to the direction of contraction. These units have variable elastic material properties, such as Young's modulus, Poisson ratio and  
10 density. Furthermore, the units can be separated by contact surfaces that allow them so slide along these faults, depending on a selected coefficient of friction.

The model results indicate, that a density contrast or the variation of the Poisson's ratio alone sparsely rotates the horizontal stress orientation ( $\leq 17^\circ$ ). Conversely, a contrast of the Young's modulus allows significant stress rotations in the order of up to  $78^\circ$ ; not only areas in the vicinity of the material transition are affected by that stress rotation. Stress rotation clearly decreases  
15 for the same stiffness contrast, when the units are separated by low friction discontinuities ( $19^\circ$ ). Low friction discontinuities in homogeneous models do not change the stress pattern at all, away from the fault; the stress pattern is nearly identical to a model without any active faults. This indicates that material contrasts are capable of producing significant stress rotation for larger areas in the crust. Active faults that separates such material contrasts have the opposite effect, they rather compensate stress rotations.

## 1 Introduction

The knowledge growth of the in-situ stress tensor in the Earth's crust is an important topic for a better understanding of the endogenic dynamic, seismic hazards or the exploitation of the underground. Therefore, several methods have been developed



to estimate both, the stress orientation or the stress magnitude. Stress orientation data are compiled globally in the World Stress  
25 Map database (Heidbach et al., 2010, 2018; Sperner et al., 2003; Zoback et al., 1989; Zoback, 1992). Based on such data  
compilations, it was assumed, that patterns of stress orientation on a regional scale are more or less consistent within tectonic  
plates (Coblentz and Richardson, 1995; Klein and Barr, 1986; Müller et al., 1992; Richardson et al., 1979).

The plate-wide pattern is overprinted on a regional scale by the current collisional systems. Recent examples in Europe are  
the Alps (Reinecker et al., 2010), the Apennines (Pierdominici and Heidbach, 2012) or the Carpathian Mountains (Bada et al.,  
30 1998; Müller et al., 2010). Closely related to that are inhomogeneities of crustal thickness, density and topography (Artyushkov,  
1973; Ghosh et al., 2009; Humphreys and Coblentz, 2007; Naliboff et al., 2012). It was suggested, that remnant stresses  
due to old plate tectonic events are able to overprint stress orientation on a regional scale (e.g. Eisbacher and Bielenstein,  
1971; Richardson et al., 1979; Tullis, 1977). Such old basement structures also provide geomechanical inhomogeneities and  
discontinuities, which have the potential to disturb the stress field. However, pre-Cenozoic orogens (or 'old' suture zones),  
35 often covered and hidden by (thick) sediments, and were rarely indicated to cause significant stress rotation. In many cases it  
is the opposite: old orogens have apparent no impact on the present-day crustal stress pattern, e.g. the Appalachian Mountains  
(Evans et al., 1989; Plumb and Cox, 1987) or Fennoscandia (Gregersen, 1992). Deviations from the assumed stress pattern  
(stress rotations) are observed recently in several regions, such as in Australia, Germany or Northern America (Heidbach  
et al., 2018; Reiter et al., 2015; Lund Snee and Zoback, 2018, 2020). However, these effects can only partly explained by the  
40 topography or lithospheric structures.

Complex stress pattern in central-western Europe was a subject of several numerical investigations in the last decades  
(Grünthal and Stromeier, 1986, 1992, 1994; Gölke and Coblentz, 1996; Goes et al., 2000; Marotta et al., 2002; Kaiser et al.,  
2005; Jarosiński et al., 2006). These 2-D models was able to reproduce some of the observed stress pattern, applying variable  
elastic material properties or discontinuities. However, the drawback of 2-D models are the limitation, that they have to integrate  
45 topography, crustal thickness and stiffness to one property; furthermore, they overestimate horizontal stresses (Ghosh et al.,  
2006). None of such studies compared the impact of the influencing factors separately.

In order to address the question, which properties are able to cause substantial stress rotations away from the material  
transition or a discontinuity, simple generic models will be used. They are inspired by the crustal structure and the stress pattern  
in the German Central Uplands, where the  $S_{Hmax}$  orientations is about  $150^\circ$ . This is in contrast to a north-south orientation ( $0^\circ$ )  
50 of  $S_{Hmax}$  to the north and to the south of the uplands (Fig. 1, Reiter et al., 2015). The basement structures there are striking  
about  $30^\circ$ , which is perpendicular to the observed  $S_{Hmax}$  orientation. The influence of the structures will be tested with variation  
of the Young's modulus, the Poisson's ratio, the density and low friction discontinuities, which separates the crustal blocks.  
Each property is tested separately first to avoid interdependencies; possible interactions are tested afterward.



## 2 Stress in the Earth crust

### 55 2.1 Sources of crustal stresses

The major contribution of stresses in crustal Earth is gravity acceleration. The acting body force is a function of density, the effective gravity and depth. The second major driver are the forces propelling plate tectonics. Plate boundary forces were identified and derive deviatoric stresses (e.g. Bott and Kusznir, 1984; Chapple and Tullis, 1977; Forsyth and Uyeda, 1975; Richardson, 1992; Zoback et al., 1989). The visible products of that are collisional zones or orogens, having a significant topography and a crustal root, which are able to overprint crustal stress pattern on a regional scale, like the fan shape stress pattern in the western and northern foreland of the Alps (Kastrup et al., 2004; Reinecker et al., 2010). There are several other features in the continental crust, which are also able to bias stress pattern on a local or regional scale. The most of these features are a product of previous geodynamical processes, such as passive continental margins, sedimentary basins, density/gravity anomalies, topography, crustal roots, etc.

65 A systematic classification was developed to range the manifold stress sources, depending on their spatial coverage in first, second and third order stress sources (Heidbach et al., 2007, 2010, 2018; Zoback et al., 1989; Zoback, 1992). First order stress sources extend over a distance of >500 km, which is larger than the thickness of the lithosphere, second order stress sources extend over a distance of 100–500 km, which is approximate the same thickness like the lithosphere, and third order stress sources extend over an distance of <100 km, which is smaller than the thickness of the lithosphere. Second and third order stress sources are able to disturb overall stress orientation trend from regional through local to reservoir scale (Heidbach et al., 70 2007, 2010, 2018; Müller et al., 1997; Tingay et al., 2005; Zoback, 1992; Zoback and Mooney, 2003).

First order stress sources next to gravity are plate boundary forces: ridge push, slab pull (Bott and Kusznir, 1984; Forsyth and Uyeda, 1975; Richardson and Reding, 1991; Richardson, 1992; Zoback and Zoback, 1981; Zoback et al., 1989; Zoback, 1992), trench suction (Elsasser, 1971), gravitational potential energy (GPE) which is related to the inhomogeneous topography and mass distribution in the lithosphere (Ghosh et al., 2009; Humphreys and Coblenz, 2007; Naliboff et al., 2012) and basal drag or tractions originating from mantle convection (Adams and Bell, 1991; Becker and Faccenna, 2011; Ghosh et al., 2013; Gough, 1984; Lithgow-Bertelloni, 2004; McGarr, 1982; Steinberger et al., 2001).

Second order stress sources are lithospheric flexure due to isostatic compensation or sediment loading on continental margins (Bott and Dean, 1972), membrane stress (Bott and Kusznir, 1984; Turcotte, 1974b) seamount loading, upwarping ocean-ward of the trench (Bott and Kusznir, 1984; Turcotte and Oxburgh, 1973; Walcott, 1970; Zoback, 1992), localized lateral density contrasts/buoyancy forces (Artyushkov, 1973; Bott and Dean, 1972; Fleitout and Froidevaux, 1982), lateral strength contrasts or anisotropy of material properties, topography (Bott and Kusznir, 1984), continental rifting, large fault zones, lateral contrasts of heat production (hydrothermal, volcanic) (Bott and Kusznir, 1979), tensile stress due to cooling of (oceanic) lithosphere (Bott and Kusznir, 1984; Turcotte and Oxburgh, 1973; Turcotte, 1974a), flexural stresses due to deglaciation (Carlsson and Olsson, 85 1982; Stein et al., 1989; Wu and Johnston, 2000) and mass re-distribution on the surface (sedimentation and erosion processes: Bott and Kusznir, 1984; Haxby and Turcotte, 1976; Turcotte and Oxburgh, 1976).



Third order stress sources are local density- or strength contrasts, internal basin geometry, basal detachments, active faults, remnant stresses as a result of ancient tectonic forces (Eisbacher and Bielenstein, 1971; Richardson et al., 1979; Tullis, 1977) and incised valleys (Savage and Swolfs, 1986). Furthermore, there are man-made increase or decrease of load (e.g. excavations or embankment dams) and downhole pressure changes (production or grouting of fluids).

## 2.2 The stress tensor

Mechanical stress describes the internal forces in solids that neighbouring particles of a continuous material apply on each other. The stress tensor is a second rank tensor, that consists of nine components from which six are independent on account of the symmetry characteristics. Three of them are normal stresses, orthogonal to each other ( $\sigma_{xx}$ ,  $\sigma_{yy}$ ,  $\sigma_{zz}$ ) and three of them are shear stresses ( $\tau_{xy}$ ,  $\tau_{xz}$ ,  $\tau_{yz}$ ). Choosing an optimal reference system, all shear stresses will disappear ( $\tau_{xy} = \tau_{xz} = \tau_{yz} = 0$ ) and the three normal stresses becomes principal stresses. Such principal stresses are independent from the reference system and are denoted in the order of magnitude:  $\sigma_1 > \sigma_2 > \sigma_3$ . For areas without topography, having lateral homogeneous material properties and density, such as sedimentary basins, it is assumed, that the vertical stress ( $S_V$ ) is a principal stress (Anderson, 1951; Brudy et al., 1997; Herget, 1973; McGarr and Gay, 1978).  $S_V$  is a cumulative product of the particular rock density, depth and gravity (Herget, 1973). Consequently, both remaining principal stresses are aligned horizontally to the Earth surface, which are the minimum- and the maximum horizontal stress ( $S_{Hmin}$  and  $S_{Hmax}$  respectively) and again orthogonal to each other. Using that simplification, the stress tensor can be described with the magnitude of  $S_V$ ,  $S_{Hmax}$  and  $S_{Hmin}$  and the orientation of  $S_{Hmax}$ . The stress regime (Anderson, 1905, 1951) are defined by the relative stress magnitudes, which are normal faulting regime ( $S_V > S_{Hmax} > S_{Hmin}$ ;  $S_V = \sigma_1$ ), strike slip regime ( $S_{Hmax} > S_V > S_{Hmin}$   $S_V = \sigma_2$ ) and thrust faulting regime ( $S_{Hmax} > S_{Hmin} > S_V$ ;  $S_V = \sigma_3$ ).

## 2.3 Indicators of stress orientation

Data indicating  $S_{Hmax}$  orientation in the Earth' crust are compiled since the 1970's (Hast, 1973; Ranalli and Chandler, 1975; Richardson et al., 1976; Sbar and Sykes, 1973), using fault plane solutions, overcoring, hydraulic fracturing or geological indicators. After recognition that borehole breakouts can be used as an indicator of  $S_{Hmax}$  orientation (Bell and Gough, 1979; Bell, 1996a; Hottman et al., 1979; Plumb and Hickman, 1985; Zoback et al., 1985), much more data became available. This led under the International Lithosphere Program to the formation of the World Stress Map (WSM) database. In the first publication, the WSM database comprised 3.574 entries (Zoback et al., 1989) and increased recently to 42.870 entries (Heidbach et al., 2018). The WSM database provide an assignment of qualities of the  $S_{Hmax}$  orientation data. The quality criteria range from A to E, where A-quality are the most reliable data, and E-quality contain ambiguous or poorly usable information.

There are three large groups of stress indicators, which are derived from different depth ranges. They are geophysical data (<40 km), borehole data ( $\ll 10$  km) and geological data from the Earth surface. The database comprises present-day  $S_{Hmax}$  orientation data, derived from single fault plane solutions (FMS), average fault plane solutions (FMA) stress inversion based on fault plane solutions (FMF), borehole breakout data (BO, BOT, BOC), hydraulic fracturing (HF, HFG, HFM, HFP), drilling induced tensile fractures (DIF), overcoring (OC) and geological indicators (volcanic alignment – GVA and fault slip analysis –



120 GFI) and other rare methods. There are many text books and publications available to delve deeply into the methods (Amadei and Stephansson, 1997; Bell, 1996a; Célérier, 2010; Richardson et al., 1979; Schmitt et al., 2012; Zang and Stephansson, 2010; Zoback, 1992).

## 2.4 Stress rotation in the upper crust

The term stress rotation is used to describe the  $S_{Hmax}$  re-orientation vertically (down-well) or rather horizontally i.e. in the map  
125 view perspective. The latter is clearly the focus of this study. All the stress sources interact with each other and therefore stress at a certain point comprises the sum of all stress sources from plate wide to very local stress sources. In the case that a regional stress pattern is disturbed by a local stress source, the difference between the resulting stress orientation and the regional stress source can be described by the angle  $\gamma$  (Sonder, 1990). The resulting (counter)-clockwise rotation ( $\gamma$ ) can be substantial and can last in a change of the stress regime (Jaeger et al., 2007; Sonder, 1990; Zoback, 1992).

130 Shallow stress orientations are mostly consistent with those data, inferred from deep focal mechanism, and therefore a vertical uniform stress field in the brittle crust is assumed (Heidbach et al., 2018; Zoback et al., 1989; Zoback, 1992). However, systematic stress rotations are observed within deep wells (Schoenball and Davatzes, 2017; Zakharova and Goldberg, 2014). This is in particular observed and expected as a result of decoupling by evaporites (e.g. Cornet and Röckel, 2012; Röckel and Lempp, 2003; Roth and Fleckenstein, 2001), or man-made activities in the underground (e.g. Martínez-Garzón et al., 2013;  
135 Müller et al., 2018; Ziegler et al., 2017). However, both is not a subject of that study.

## Density contrast and topography

Variability of density within the crust or lithosphere have a significant impact on the stress state (Artyushkov, 1973; Fleitout and Froidevaux, 1982; Frank, 1972; Ghosh et al., 2009; Humphreys and Coblenz, 2007; Naliboff et al., 2012). Assameur and Mareschal (1995) showed, that local stresses due to topography and crustal inhomogeneities are in the order of tens of MPa,  
140 which are on the similar magnitude as the plate boundary forces. Gravitational forces are also derived by surface topography (Miller and Dunne, 1996; Zoback, 1992). On top of mountains,  $S_{Hmax}$  is oriented parallel to the ridge and perpendicular at the foot of the mountain chain. Along passive continental margins, similar effects like for topography are to observe (Bell, 1996b; Bott and Dean, 1972; King et al., 2012; Stein et al., 1989; Tingay et al., 2005; Yassir and Zerwer, 1997). Sonder (1990) investigated the interaction of different regional deviatoric stress regimes ( $\sigma_D$ ) with stresses arising from buoyancy forces ( $\sigma_G$ )  
145 and observe a rotation of  $S_{Hmax}$  of up to  $90^\circ$ . According to that,  $S_{Hmax}$  rotates toward the normal trend of the density anomaly. If regional stresses are large, compared to stresses driven by a density anomaly ( $\sigma_D/\sigma_G \ll 1$ ), the influence of density anomaly is small and vice versa: If the regional stress is small, compared to the stress driven by the density anomaly ( $\sigma_D/\sigma_G \gg 1$ ), the impact of a density anomaly on the resulting stress field is large. In the case that both stress sources are on a similar level ( $\sigma_D/\sigma_G \approx 1$ ), small changes of one of the stress sources are able to change the stress regime, and therefore potentially the  
150 deformation style.



## Strength contrast

Mechanical strength describes the material behaviour under the influence of stress and strain. The focus here is on elastic material properties, characterized by the Young's modulus and the Poisson's ratio. Stress refraction between two elastic media can be calculated, but only at the interface of the two media, based on the known stress state on one side of the interface and the Young's modulus of both (Spann et al., 1994). Stress rotation due to strength contrast are e.g. reported for the Peace River Arch in Alberta (Adams and Bell, 1991; Bell and Lloyd, 1989; Fordjor et al., 1983). Potential stress rotation is confirmed by several numerical studies (Bell and Lloyd, 1989; Grünthal and Stromeyer, 1992; Mantovani et al., 2000; Marotta et al., 2002; Spann et al., 1994; Tommasi et al., 1995; Zhang et al., 1994).

## Discontinuities

Discontinuities are planar structures within or between rock units, where the shear strength is (significant) lower than that of the surrounding rock. Genetically, discontinuities can be classified into bedding, schistosity, joints and fault planes. In the context of that study the term discontinuity refers to fault planes or fault zones. Similar to the Earth surface, (nearly) frictionless faults act like a free surface in terms of continuum mechanics (Bell et al., 1992; Bell, 1996b; Jaeger et al., 2007). One of the three principal stresses must be oriented perpendicular to the frictionless fault, the two remaining ones are parallel to the discontinuity. For this reason, the stress tensor bends near a frictionless fault, depending on its orientation. Significant stress rotation in the context of faults are reported (Adams and Bell, 1991; Bell and McCallum, 1990; Mazzotti and Townend, 2010; Yale, 2003). However, Yale (2003) assumes, that stress rotation occurs several kilometres away from the fault. Small differences between the horizontal stresses increases the effect of faults on the local stress pattern, whereas large stress differences lead to more homogeneous stress pattern (Laubach et al., 1992; Yale, 2003). The impact of faults on stress rotation is investigated by numerical models (e.g. Homberg et al., 1997; Zhang et al., 1994; Tommasi et al., 1995).

## 3 Regional setting

### 3.1 Stress Orientation in Central Europe

Crustal stress data from Europe have been collected since the 1960's (e.g. Froidevaux et al., 1980; Greiner, 1975; Greiner and Illies, 1977; Hast, 1969, 1973, 1974; Kohlbeck et al., 1980; Ranalli and Chandler, 1975) and later within the framework of the World Stress Map database. These data were applied to investigate the crustal stress pattern for Western Europe (Ahorner, 1975; Carafa and Barba, 2013; Gölke and Coblenz, 1996; Klein and Barr, 1986; Müller et al., 1992), Scandinavia (Gregersen, 1992), Central Europe (Grünthal and Stromeyer, 1986, 1992, 1994), the Alps (Kastrup et al., 2004; Reinecker et al., 2010), or for the Mediterranean area (Rebaï et al., 1992). As principal  $S_{Hmax}$  orientation are identified as north-west to north-north-west in Western Europe, a slightly rotation to north-east in central Europe, a west-north-west orientation in Scandinavia and a east-west orientation in the Aegean Sea and western Anatolia.



$S_{Hmax}$  orientation in western Europe of  $145^{\circ} \pm 26^{\circ}$  deviates clockwise by about  $17^{\circ}$  (Müller et al., 1992) to the direction of absolute plate motion from Minster and Jordan (1978). This is in agreement with Zoback et al. (1989) which obtained a better fit for relative plate motion between Africa and Europa, than for absolute plate motion. As major reasons for the observed stress pattern in western and central Europe are the ridge push of the Mid-Atlantic ridge and the collisional forces along the southern plate margins are identified (Goes et al., 2000; Gölke and Coblenz, 1996; Grünthal and Stromeyer, 1986, 1992; Klein and Barr, 1986; Müller et al., 1992; Richardson et al., 1979; Zoback et al., 1989; Zoback, 1992).

A fan like stress pattern has been observed in the western Alps and Jura mountains, where  $S_{Hmax}$  in front of the mountain chain is perpendicular to the strike of the orogen. Müller et al. (1992) assumes, that these structures only locally overprints the general stress pattern. However, in the light of the recently available data, it is assumed, that the  $S_{Hmax}$  orientation is rather controlled by gravitational potential energy of the alpine topography than by plate boundary forces (Grünthal and Stromeyer, 1992; Reinecker et al., 2010). The explanation of that crustal structure are a cold, dense and slowly subsiding lithospheric root beneath the Alps (Müller and Zürich, 1984).

Stress pattern in western and central Europe has been an subject of several modelling attempts in the last three decades (Grünthal and Stromeyer, 1986, 1992, 1994; Gölke and Coblenz, 1996; Goes et al., 2000; Marotta et al., 2002; Kaiser et al., 2005; Jarosiński et al., 2006). Among other things, it was examined which factors contributes to the observed stress pattern. Investigated was the impact of a stiffness contrast in the crust (Grünthal and Stromeyer, 1986, 1992, 1994; Jarosiński et al., 2006; Kaiser et al., 2005; Marotta et al., 2002), the elastic thickness of the crust (Jarosiński et al., 2006), the stiffness contrast of the mantle (Goes et al., 2000), a lateral density contrast or topographic effects (Gölke and Coblenz, 1996; Jarosiński et al., 2006), the post-glacial rebound in Scandinavia (Kaiser et al., 2005) and activity on faults (Kaiser et al., 2005; Jarosiński et al., 2006).

Stiffness variation in the lithosphere, e.g the Teisseyre-Tornquist Zone (TTZ) or the Bohemian Massif (BM), has been identified as the major reasons for observed stress rotation in Central Europe (Goes et al., 2000; Gölke and Coblenz, 1996; Grünthal and Stromeyer, 1986, 1992, 1994; Kaiser et al., 2005; Marotta et al., 2002; Reinecker and Lenhardt, 1999). One example is the fan shaped stress pattern in the North German Basin (NGB), with a rotation of  $S_{Hmax}$  from north-west in the western part to north-east in the eastern part of the basin as a product of the TTZ, which is the boundary between the Phanerozoic Europe (Avalonia) and the much stiffer Precambrian Eastern European Craton (Baltica). However, Jarosiński et al. (2006) came to the conclusion, that active tectonic zones and topography has major effects, whereas the stiffness contrast lead only to minor effects. Post-glacial rebound does have an effect on the stress pattern in the NGB (Kaiser et al., 2005). Lateral variation of density do not have a significant impact on the stress pattern (Gölke and Coblenz, 1996), it provides only local effects. Finally, small differential stress allows significant stress rotation (Grünthal and Stromeyer, 1992).

### 3.2 Basement structures in Germany

The Variscan orogen is a product of the late-Paleozoic collision of the plates Gondwana and Avalonia (Laurussia) in late Devonian to early Carboniferous time, which lead to closure of the Rheic Ocean (Matte, 1986), and finally the formation of the super-continent Pangea. Despite the fact, that the European Varicides are well investigated in the last century and decades (e.g.

215 Franke, 2000, 2006; Kroner et al., 2007; Kroner and Romer, 2013), it is for example still a matter of debate, whether several microplates have been amalgamated in-between or not.

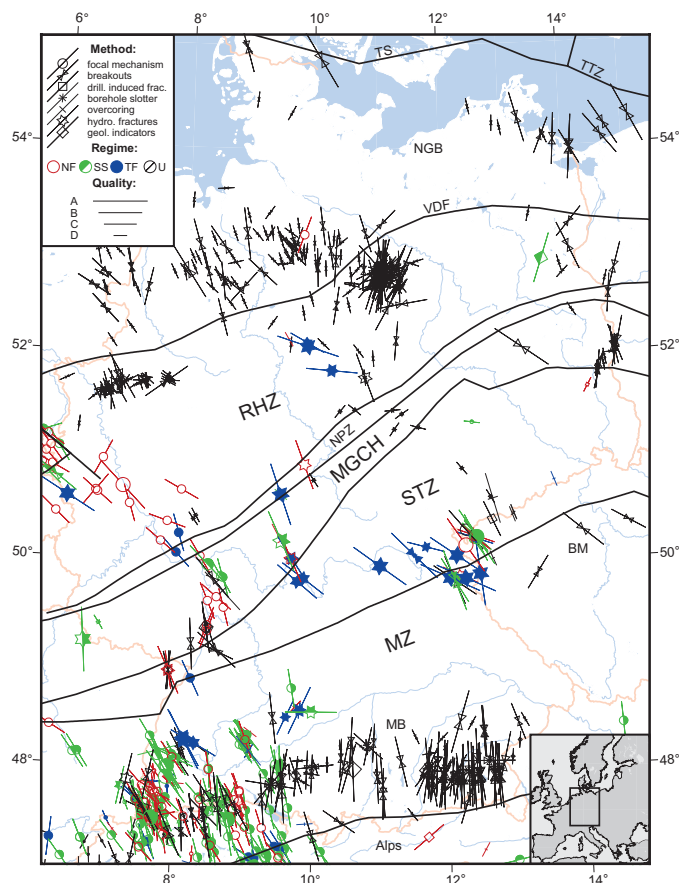


**Figure 1.** Stress orientation in the German Central Uplands with the basement structural elements, political boundaries (red) and the major river (blue). Bars represent orientations of maximum horizontal compressional stress ( $S_{Hmax}$ ), line length is proportional to quality. Colours indicate stress regimes, with red for normal faulting (NF), green for strike-slip faulting (SS), blue for thrust faulting (TF), and black for unknown regime (U). The Variscan basement structures introduced by Kossmat (1927) are visualized; the regional segmentation is: MZ = Moldanubian Zone, BM = Bohemian Massif, MGCH = Mid-German Crystalline High, NPZ = Northern Phyllite Zone, RHZ = Rheno-Hercynian Zone, STZ = Saxo-Thuringian Zone, and VDF = Variscan Deformation Front. Other structures are: TS = Thor Suture, TTZ = Teisseyre-Tornquist Zone, NGB = North German Basin, MB = Molasses Basin; (Redrawn after Franke, 2014; Grad et al., 2016).

Kossmat (1927) published the structural zonation of the European Variscides, which is still widely used (Fig. 1). The parts north-west of the Rhenic Suture Zone are the Rheno-Hercynian Zone (RHZ) with the sub-unit of the Northern Phyllite Zone (NPZ), both with Laurussian origin. South-east of the suture zone are the Mid-German Crystalline High (MGCH), the Saxo-Thuringian Zone (STZ) and the Moldanubian Zone (MZ); all where exclusively part of Gondwana, except the MGCH.



The Rheno-Hercynian Zone (RHZ) is exposed in the Rhenish Massif, in the Harz mountains and in the Felchting horst. Dominant are Devonian to lower Carboniferous clastic shelf sediments (Franke, 2000; Franke and Dulce, 2017). These low metamorphic slates, sandstones, greywacke and quartzite are supplemented with continental and oceanic volcanic rocks, reef limestones and a few older gneisses. Further to the north of the RHZ are the sub-variscan foreland deposits, consisting of clastic  
225 sediments and coal seams.

The Northern Phyllite Zone (NPZ) is uncovered at the southern edge of the low mountain ranges Hunsrück, Taunus and eastern Harz. Petrological it is probably the greenschist facies equivalent (Oncken et al., 1995) of the Rheno-Hercynian shelf sequence (Klügel et al., 1994), consisting of meta-sediments and within-plate metavolcanic rocks (Franke, 2000).

The Mid-German Crystalline High (MGCH) is open in the Palatinate Forest, Odenwald, Spessart, Kyffhäuser, Ruhla Chry-  
230 talline (Thuringian Forest) and Flechting Horst. It has been interpreted previously as magmatic arc of the Soxo-Thuringian Zone. But Oncken (1997) assumes that the MGCH is composed from both, Saxo-Thuringian and Rheno-Hercynian rocks. Composition and metamorphic grade varies considerably along-strike of the MGCH (Franke, 2000). It consists of late-Paleozoic sediments, meta-sediments, volcanic rocks, granitoides, gabbros, amphibolite and gneisses.

The Saxo-Thuringian Zone (STZ) is exposed in the Thuringian-Vogtlandian Slate Mountains, Fichtel Mountains, Ore Moun-  
235 tains, Saxonian Granulite Massif, Elbe Valley Slate Mountains, and the Lausitz. It consists of Campro-Ordovician mafic and felsic magmatic rocks, late Ordovician to early Carboniferous marine and terrestrial sediments (Franke, 2000; Linnemann, 2004). These rocks underwent metamorphic overprint up to the early Carboniferous with different metamorphism stage up to eclogite- or granulite facies. These units are interspersed by late- or post-orogenic granites.

The Moldanubian Zone (MZ) is exposed in the Bohemian Massif, the Bavarian Forest, the Münchberg Gneiss Massif, the  
240 Black Forest and the Vosges. They consist of mostly high grade metamorphic crystalline rocks (gneisses, granulite, migmatite) and variscan granites (Franke, 2000).

## 4 Model set-up

### 4.1 Model dimension

The chosen model geometry is inspired by the geometrical situation in the German Central Uplands (Fig. 1), but the overall  
245 intention is a generic model. To make it easy to understand, compass directions are used for model description. The model geometry has a north-south extend of 400 km and 300 km in east-west orientation, with a thickness of 30 km (Fig. 2). In the centre of the model, three diagonal units having a width of 50 km are oriented 30° counter-clockwise from east-west. For each of the three unit, separate material properties can be applied. The most northern and southern block has always basic material properties. Furthermore, a model variation is generated, where the units are separated by contact surfaces, allowing free slip  
250 depending on a chosen friction coefficient.

The lateral element resolution is about 3 km consisting primary of hexahedrons and some wedge elements (degenerated hexahedrons). Element resolution into depth ranges from 0.44 km near the surface to about 3.4 km at greatest model depth. The total amount is about 166 k elements; the model version having contact surfaces uses 1725 contact elements along each contact

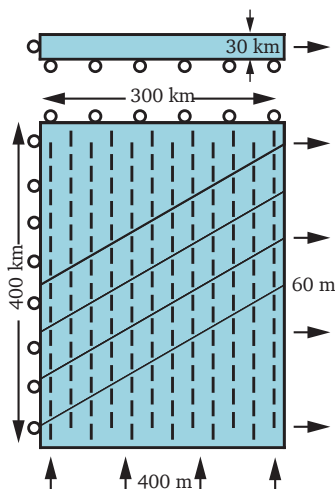


**Figure 2.** Basic model with the applied boundary conditions. The model has a lateral extend of  $300 \times 400$  km and a thickness of 30 km. The model consists of five connected units; here visualized in blue, they have all the basic material properties (Tab. 1). The boundary conditions ban motion in x-direction on the western side, in y-direction on the northern side and in z-direction at the model base. A push of 400 m from the south and a pull of 60 m to the east is applied. The resulting  $S_{Hmax}$  orientation (north-south) in a depth of 1000 m are illustrated by the black bars. The four diagonal boundaries can be used as discontinuities.

surface. The mesh is generated using HyperMesh® v.2019. The equilibrium of forces (body forces and boundary condition) is  
 255 estimated numerically using the Abaqus®/Standard v.6.14-1 finite element software.

## 4.2 The Finite Element Method

The finite element method (FEM) is used since the 1950's to investigate the stability of structures such as wings of an airplane (Turner et al., 1956). Since the 1970's the method has been introduced in geoscience, to investigate the stress orientation in the Earth crust on certain structures using generic 2-D models (Stephansson and Berner, 1971), or to investigate the stress  
 260 orientation pattern for large regions (Richardson et al., 1976; Grünthal and Stromeier, 1986). The usage of 3-D FEM models, to investigate the stress state in the crust is now a well-established technique (e.g. Buchmann and Connolly, 2007; Hergert and Heidbach, 2011; Hergert et al., 2015; Reiter and Heidbach, 2014). The major reason that complex 2-D or 3-D models can be computed, is the opportunity to use unstructured meshes.

The method in general computes the equilibrium of stresses with forces (boundary conditions), body forces (gravity) and  
 265 used material properties. Numerically, this is implemented by partial differential equations:

$$\frac{\delta\sigma_{ij}}{\delta x_j} + \rho x_i = 0 \quad (1)$$

where  $\delta\sigma_{ij}$  is the variation of total stress,  $\delta x_j$  the geometrical change, and  $\rho x_j$  represents the weight of the rock section ( $\rho =$  density). The previously described balance of forces is well described by the linear elastic material properties (Hooke's law).



Two material properties, the Young's modulus ( $E$ ) and the Poisson's ratio ( $\nu$ ) are essential; density is not absolutely necessary  
270 but enables that body forces act. The stress state in this study will be calculated based on defined displacement boundary  
conditions.

### 4.3 Material properties

The main subject of that study is to investigate the impact of the variation of elastic rock properties, density and friction along  
faults on stress orientation in the upper crust. To do this each parameter is tested individually. Figure 3 visualize the range of  
275 density ( $\rho$ ), Young's modulus ( $E$ ) and Poisson's ratio ( $\nu$ ) of representative rocks, taken from a textbook (Turcotte et al., 2002).

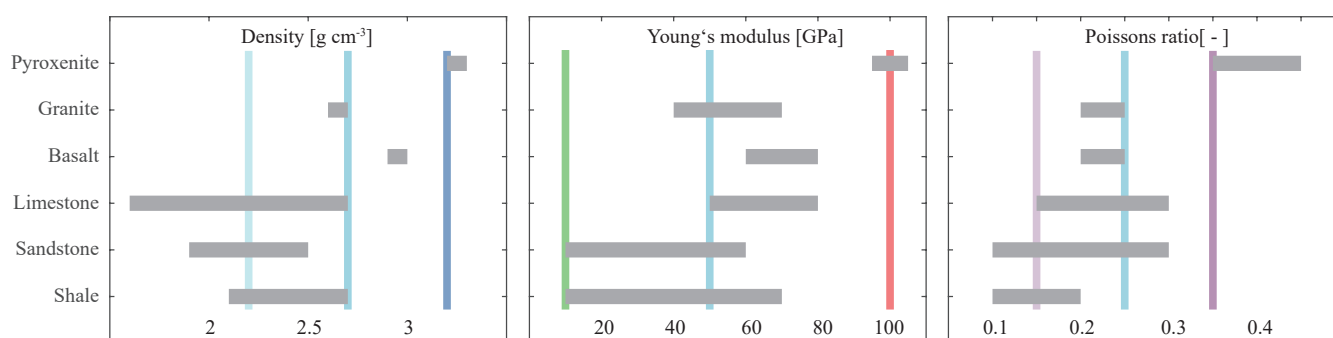


**Figure 3.** Selection of common elastic rock properties (Young's modulus and Poisson's ratio) and density (Turcotte et al., 2002). Coloured vertical bars indicate applied material properties.

The basic material for this investigation has a density of  $\rho = 2.7 \text{ g cm}^{-3}$ , a Poisson's ratio of  $\nu = 0.25$  and a Young's modulus  
of  $E = 50 \text{ GPa}$ . Such a material could represent for example granite or limestone. Based on this basic material, always a lower  
and higher material value is defined (Tab. 1), which is within the range of common rocks properties (Fig. 3). The material with  
a low density ( $\rho = 2.2 \text{ g cm}^{-3}$ ) may represent sediments (sandstone, limestone, shale etc.), where the high density material  
280 ( $\rho = 3.2 \text{ g cm}^{-3}$ ) could represent a rock from the lower crust or the upper mantle. A low Poisson's ratio ( $\nu = 0.15$ ) may  
represent sediments (sandstone or shale), and a high Poisson's ratio ( $\nu = 0.35$ ) could represent ultramafic rock. Soft material  
with a low Young's modulus ( $E = 10 \text{ GPa}$ ) may represent sediments, pre-damaged or weathered rock. Again ultramafic rock  
is an example for a stiff rock, having a large Young's modulus ( $E = 100 \text{ GPa}$ ).

Laboratory rock experiments in the past delivered friction coefficients of about  $\mu = 0.6$  to  $0.85$  (Byerlee, 1978). However,  
285 recent investigations using realistic slip rates for earthquakes decreased estimated friction coefficients by one order of mag-  
nitude up to  $\mu < 0.1$  (Di Toro et al., 2011). Faults are represented by cohesionless contact surfaces in the models. The used  
friction coefficients are 0.1, 0.2, 0.4, 0.6, 0.8 and 1.0, which finally covers slow- and fast slip rates as well.



**Table 1.** Material properties and densities which has been used in the models. Bold numbers indicate the properties used, which differ from those of the basic material.

Name	Young's Modulus [GPa]	Poisson's ratio [-]	Density [g cm <sup>-3</sup> ]
Basic material (B)	50	0.25	2.7
Low Density (g)	50	0.25	<b>2.2</b>
High Density (G)	50	0.25	<b>3.2</b>
Low Poisson (p)	50	<b>0.15</b>	2.7
High Poisson (P)	50	<b>0.35</b>	2.7
Low Stiffness (e)	<b>10</b>	0.25	2.7
High Stiffness (E)	<b>100</b>	0.25	2.7
Upper Mantle	<b>130</b>	0.25	<b>3.25</b>

#### 4.4 Boundary conditions

The overall  $S_{Hmax}$  orientation on an imagined profile along longitude 11° (Fig. 1) displays a north-south orientation in the North German Basin (NGB) and in the Molasses Basin (MB) north of the Alps, except the Variscan basement units in-between. According to that, a north-south orientation of  $S_{Hmax}$  is intended for the basic model. To define appropriate boundary conditions (lateral strain), results from a virtual well in the model centre are compared with data from deep wells. Several strain scenarios where applied to the pre-stressed basic model. An extension of 60 m ( $\epsilon_x = 0.02$ ) in east-west direction and a shortening of 400 m ( $\epsilon_y = -0.1$ ) in north-south direction (Fig. 2) provides a good fit to stress magnitudes from selected deep wells (Brudy et al., 1997; Hickman and Zoback, 2004; Lund and Zoback, 1999). By fitting the data, the focus was more on the observed  $S_{Hmin}$  magnitudes and to a less extend on the  $S_{Hmax}$  magnitudes. The latter are less reliable, as they are usually not measured; they are calculated on the basis of several assumptions.

#### 4.5 Model scenario's

The model geometry consists of five units (Fig. 2). The northern- and southern most block uses always the basic material properties (Tab. 1). In between are three diagonal units, where material properties or friction properties will be varied. The numerical lower (L) or higher (H) material properties regarding the basic material (B) will be varied in the following way: LLL, HHH, LBL, BLB, etc. When the model geometry mimics discontinuities using contact surfaces, all contacts have the same friction coefficient. The visualization takes place in the following way, where 'l' indicates the contact. For example, HLH with four contacts is lHlHl. The  $S_{Hmax}$  orientation will be visualized for a depth of 1000 m below the surface using a pre-defined pattern, where the lateral distance to the material transition or discontinuity is >12.5 km, as far field effects are the major interest of that study.

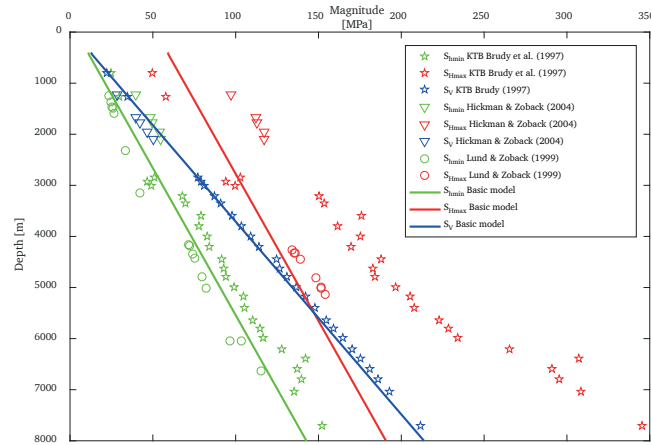


**Figure 4.** Stress magnitudes are plotted versus depth. The stress components from the virtual well in the centre of the basic model are shown by the lines, using the boundary conditions illustrated in Fig. 2. Due to the applied initial stress conditions, the stress regime switches from thrust faulting in a depth of around 400 m below the surface to strike slip faulting, and finally to a normal faulting regime in a depth greater than 5500 m. Additionally, published stress magnitude data are shown for comparison (Brudy et al., 1997; Hickman and Zoback, 2004; Lund and Zoback, 1999).

The variation of the density, the Poisson's ratio, the Young's modulus, the friction coefficient will be tested first. Additionally, the Variation of Young's modulus using low friction contacts, a modification of the model with an additional 30 km stiff mantle and a thinner model, having a thickness of only 10 km will be tested. The latter are only mentioned in the discussion.

## 310 5 Resulting stress rotation

### 5.1 Density influence

To identify the influence of a density variation, the basic density ( $\rho = 2.7 \text{ g cm}^{-3}$ ) in blue are varied using a small density ( $g: \rho = 2.2 \text{ g cm}^{-3}$ ), which is coloured in light blue and a large density ( $G: \rho = 3.2 \text{ g cm}^{-3}$ ), which is dark blue in Fig. 5.

The low density anomaly (ggg) result in a slightly counter-clockwise ( $-6^\circ$ )  $S_{Hmax}$  orientation in the basic material near the anomaly (Fig. 5). Within the low density units near the basic material, nearly no rotation is to observe ( $-1^\circ$ ), but turns more counter-clockwise ( $-8^\circ$ ) in the centre of the material anomaly. The angular variation of  $S_{Hmax}$  crossing the units is in the order of  $7^\circ$ . The high-density anomaly (GGG) results in a slightly clockwise rotation ( $+7^\circ$ ) in the basic material near the anomaly. In the high density unit near the basic material,  $S_{Hmax}$  is minimally influenced ( $+1^\circ$ ), but rotates further clockwise ( $+12^\circ$ ) in the centre of the anomaly. Based on that, the variation across the units is about  $11^\circ$ . The models with mixed densities in the  
 315  
 320  
 three units show a clockwise rotation ( $+10^\circ$ ) of  $S_{Hmax}$  within the lighter material next to the more dense units. The high density units show a counter-clockwise rotation ( $-7^\circ$ ) next to the low density unit; therefore, the total variation of  $S_{Hmax}$  is  $17^\circ$ .

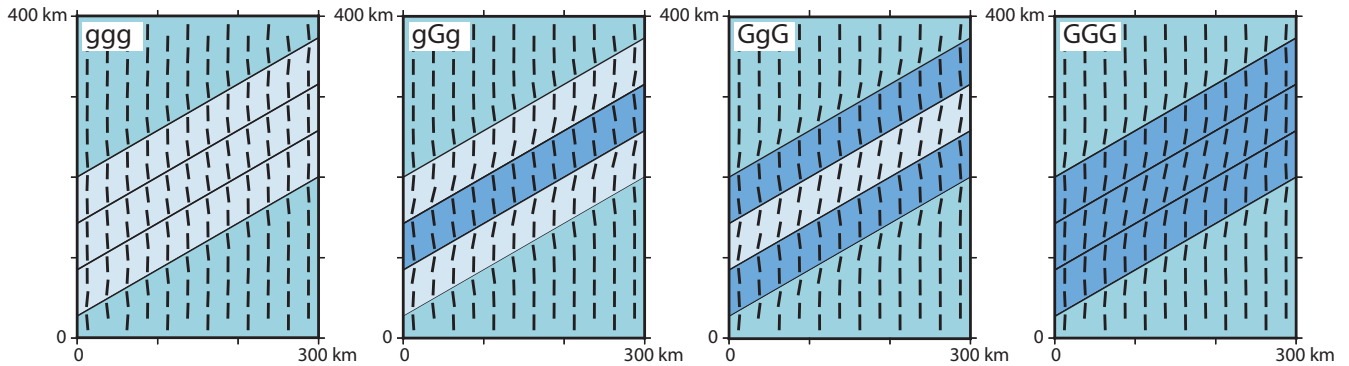


**Figure 5.** Influence of density on the stress orientation. Black bars represents the orientations of the maximum horizontal compressional stress ( $S_{Hmax}$ ) at a depth of 1000 m. Colours indicate the used material properties. The blue area uses the basic material properties ( $\rho = 2.7 \text{ g cm}^{-3}$ ), the light blue material uses a lower density (g:  $\rho = 2.2 \text{ g cm}^{-3}$ ), the dark blue a larger density (G:  $\rho = 3.2 \text{ g cm}^{-3}$ ).

In general,  $S_{Hmax}$  is oriented parallel to the anomaly in low density units and perpendicular to the anomaly in the large density units. In the centre of the low density units (ggg), the stress orientation becomes perpendicular to the overall structure. For the centre of the high density units (GGG) happens the opposite,  $S_{Hmax}$  becomes parallel to the spacious structure.

## 325 5.2 Influence of the Poisson's ratio

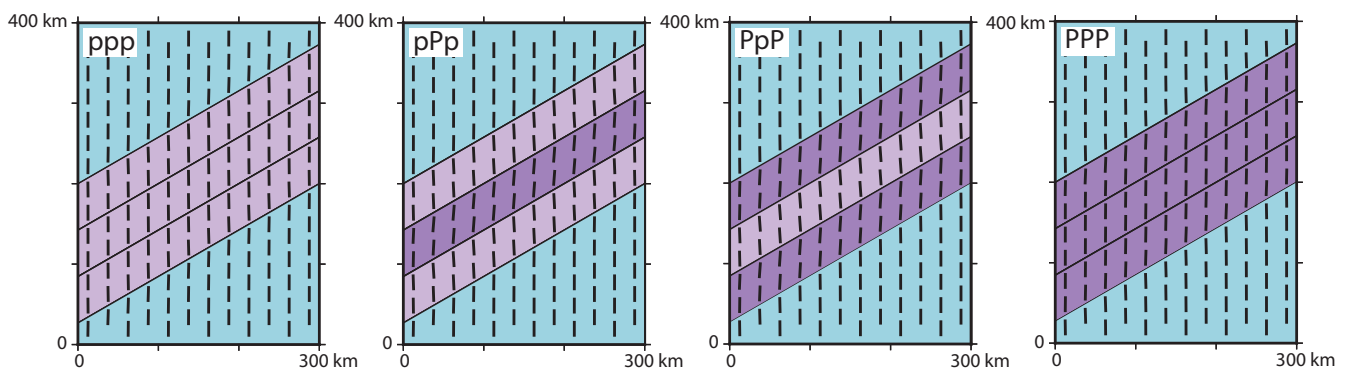


**Figure 6.** Influence of the Poisson's ratio on the stress orientation. Black bars represents the orientations of the maximum horizontal stress ( $S_{Hmax}$ ) at a depth of 1000 m. Colours indicate the used material properties. The blue area uses the basic material properties ( $\nu = 0.25$ ), the light purple material uses a low Poisson's ratio (p:  $\nu = 0.15$ ), where the dark purple material have a large Poisson's ratio (P:  $\nu = 0.35$ ).

The influence of the Poisson's ratio on the stress rotation is tested by variation of the basic Poisson's ratio ( $\nu = 0.25$ ) using a lower one (p:  $\nu = 0.15$ ) in light purple and a larger one (P:  $\nu = 0.35$ ) in dark purple.

The models with only a lower (ppp:  $-1.5^\circ$ ) and only a higher Poisson's ratio (PPP:  $+2.2^\circ$ ) shows only little  $S_{Hmax}$  rotation (Fig. 6). Mixed models with largest Poisson's ratio variation (pPp and PpP) have some counter-clockwise rotation in the low



330 Poisson's ratio units ( $-3.0^\circ$ ) and a clockwise rotation in the high Poisson's ratio units ( $+4.2^\circ$ ). Therefore, the total variance of  $S_{Hmax}$  is about  $7.5^\circ$ .

### 5.3 Impact of Young's modulus

The impact of the Young's modulus variation is investigated taking a basic material (B:  $E = 50$  GPa) in contrast to a softer material (e:  $E = 10$  GPa) in green and a stiffer material (E:  $E = 100$  GPa) in red (Fig. 7).

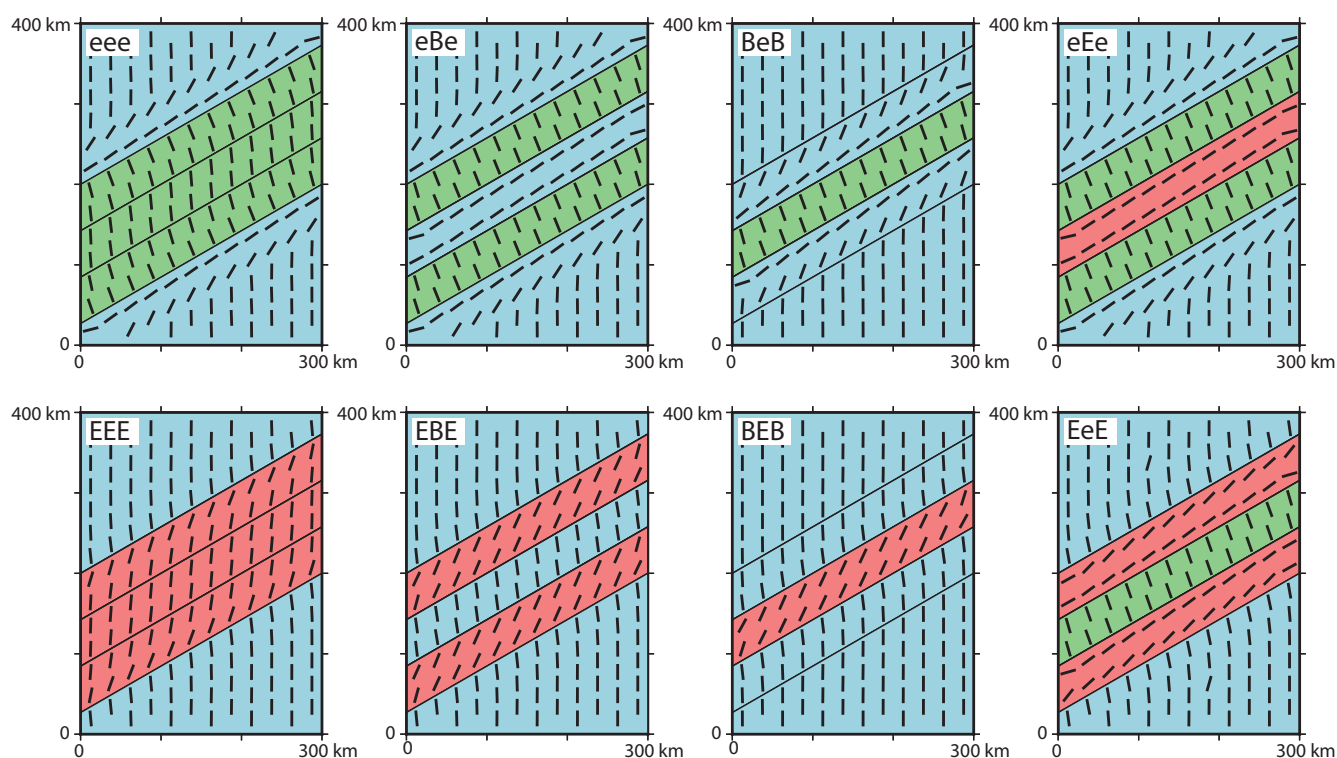


**Figure 7.** Influence of Young's modulus on the stress orientation. Black bars represent the orientations of the maximum horizontal stress ( $S_{Hmax}$ ) at a depth of 1000 m. Colours indicate the used Young's modulus; the blue area uses the basic material properties (B:  $E = 50$  GPa), the green material uses a low Young's modulus (e:  $E = 10$  GPa), where the red material have a large Young's modulus (E:  $E = 100$  GPa).

335 The models with the soft units (eee, eBe and BeB) exhibit a strong clockwise  $S_{Hmax}$  rotation ( $+56^\circ$ ) in the units with the basic material and a counter-clockwise rotation in the softer units ( $-22^\circ$ ) near the material transitions (Fig. 7). Within the models having three soft units (eee) the  $S_{Hmax}$  orientation decreases to  $-5^\circ$  in the centre of the units. That means within the soft units  $S_{Hmax}$  variation is considerable ( $17^\circ$ ). The total variation is  $78^\circ$ . The models with the stiff units (EEE, EBE and BEB) exhibits a gentle counter-clockwise rotation in the units with the basic material ( $-5.5^\circ$  to  $-7^\circ$ ) next to the stiff units. Within  
 340 the stiff units, a significant clockwise rotation ( $+20^\circ$  to  $+25^\circ$ ) is apparent next to the basic units. The model having three stiff units (EEE) the  $S_{Hmax}$  orientation decreases to ( $+5^\circ$ ) in the centre. This is a  $S_{Hmax}$  variation of considerable  $15^\circ$  within the



stiff units. The total variation is  $31^\circ$ . For the models with alternating units with soft and stiff material (EeE and eEe), the soft units exhibits a counter-clockwise  $S_{Hmax}$  rotation ( $-19^\circ$  to  $-22^\circ$ ), where the stiff units displays a clockwise rotation ( $+53^\circ$  to  $+56^\circ$ ). Consequently the total variation between the soft and stiff units is  $72^\circ$  to  $78^\circ$ . The general observation is, that next to  
345 the material transition,  $S_{Hmax}$  rotates perpendicular to the anomaly for the weak units and parallel for the stiff units.

#### 5.4 Influence of faults

Several models with the basic material properties separated by three discontinuities (|B|B|B|) having a friction coefficient ( $\mu$ ) from 0.1 to 1 are tested. The low friction coefficient ( $\mu = 0.1$ ) leads to a counter-clockwise  $S_{Hmax}$  rotation of only  $-3^\circ$  (Fig. 8). By increasing the friction coefficient to  $\mu = 0.2$ , the  $S_{Hmax}$  rotation is  $-2^\circ$ , for  $\mu = 0.4$ ,  $S_{Hmax}$  rotation is  $-1^\circ$ . For larger  
350 friction coefficients the  $S_{Hmax}$  rotation is below  $-1^\circ$ . As the  $S_{Hmax}$  rotation is too small for a visual differentiation, only the  $\mu = 0.1$  model is shown in Figure 8.

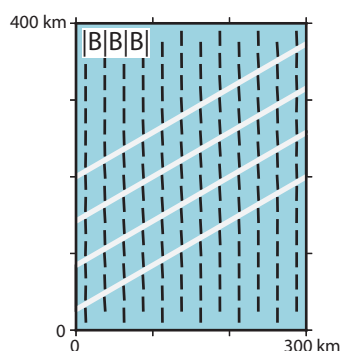


**Figure 8.** Influence of faults on the far field stress orientation. Black bars represents the orientation of the maximum horizontal compressional stress ( $S_{Hmax}$ ) at a depth of 1000 m. All areas have the basic material properties (Tab. 1.). White lines indicate cohesionless discontinuities (faults). The model using a friction coefficient of  $\mu = 0.1$  along the three discontinuities is shown. The other models with a larger friction coefficient (up to 1 and larger) have similar results, they are waived out because of the visual similarity.

#### 5.5 Stiffness variation combined with low friction faults

The interaction of a significant Young's modulus difference is tested in combination with a low friction coefficient ( $\mu = 0.1$ ) along all four discontinuities. The model with three stiff units (|E|E|E|) provides only little counter-clockwise rotation ( $-4^\circ$ ) in  
355 the basic material near the material transition (Fig. 9). Similar clockwise rotation occur in the stiff units ( $+4^\circ$ ) near the material transition, which decreases to the material centre ( $+1^\circ$ ). However, the total  $S_{Hmax}$  variation of about  $8^\circ$ .

The model with the soft units and the low friction discontinuities (|e|e|e|) displays significant larger rotation then for the stiff units. Clockwise rotation of  $+19^\circ$  occurs in the basic material and counter-clockwise rotation of  $-13^\circ$  in the soft units. This decreases toward the centre of the soft units ( $-9^\circ$ ). Both rotations together result in about  $32^\circ$ .

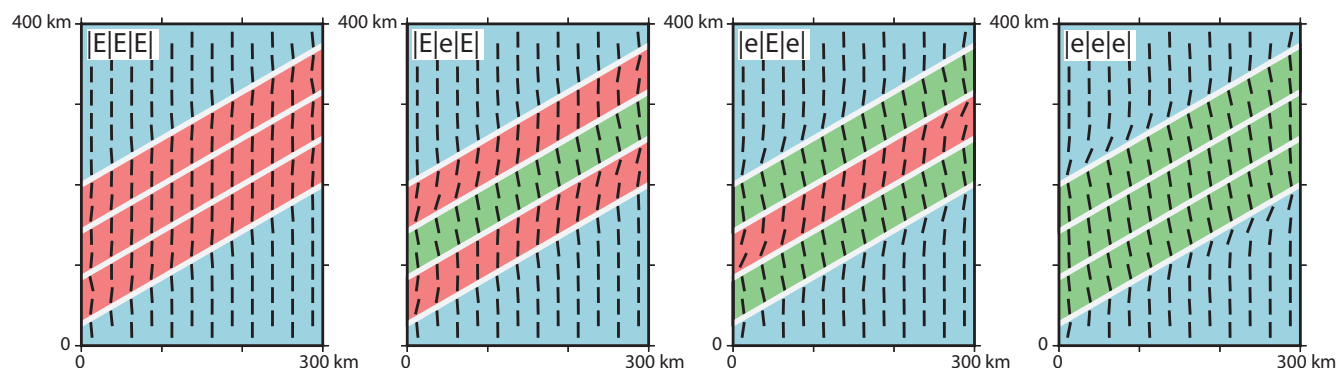


**Figure 9.** Influence of Young's modulus in interaction with low friction faults on the far field stress orientation. Black bars represents the orientations of the maximum horizontal stress ( $S_{Hmax}$ ) at a depth of 1000 m. Colours indicate the used material properties. The blue area uses the basic material properties, the green material uses a low Young's modulus, where the red material has a larger Young's modulus, see Tab. 1. White lines indicate cohesionless discontinuities (faults) with a friction coefficient of  $\mu = 0.1$ .

360 In the models with the alternating stiffness with the low friction discontinuities (|E|e|E| and |e|E|e|) provides a counter-clockwise rotation of about  $-10^\circ$  to  $-12^\circ$  in the soft units. Within the stiff units, the  $S_{Hmax}$  orientation is in the range of  $+2^\circ$  to  $+7^\circ$ . The total variation is up to  $19^\circ$ .

## 6 Discussion

### 6.1 Model simplification

365 This study investigates the influence of elastic material properties, density and the friction coefficient on vertical faults on the orientation of  $S_{Hmax}$ . Although the model may be inspired by a particular region, but the goal is to gain a better understanding of the interaction of the variable material properties on the stress orientation ( $S_{Hmax}$ ). The focus is not on stress rotation close ( $<5$  km) to the material transition or discontinuity, the priority is on the far field effects. Fore sure it is really unlikely that such constant materials with such a thickness exists somewhere in the crust. Not only the geometry is a strong simplification, but  
370 also the neglect of various rheological processes in the crust by applying linear-elastic material laws is a strong simplification. However, the overall geometry seems reasonable, as the brittle domain or elastic thickness of the crust ( $Te$ ), which is a measure of the integrated strength of the lithosphere, is in the order of 30 km and more in central Europe (Tesauro et al., 2012). The Moho depth in central Europe is also about 30 km (Grad and Tiira, 2009). Jarosiński et al. (2006) for example used a range of  $Te = 30-100$  km for their model of central Europe.

375 The models were tested with an additional stiff mantle with a thickness of 30 km. This had no influence on the observed stress pattern in a depth of 1000 m depth. But the models with the same geometry and a total thickness of only 10 km resulted in much lower stress rotation. Therefore, the elastic thickness of the crust and the width of the anomaly is an important constraint



for the possible stress rotation. The depth at which the stress orientation is plotted is also important, as the stress rotation changes with depth.

## 380 6.2 Stress rotation by density contrast

The lateral variation of the density is responsible for  $S_{Hmax}$  rotation in the range of  $7^\circ$  to  $17^\circ$  (Fig. 5). In general, the  $S_{Hmax}$  rotates in the low density units slightly toward parallel to the high density unit, whereas  $S_{Hmax}$  rotates in the high density units a little bit in the direction to the low density units. Taking a broad range of sediments into account (evaporates, shale, sand- or limestone), they could have even a lower density than the used lowest value ( $\rho = 2.2 \text{ g cm}^{-3}$ ). However, sediments could  
385 reach a thickness of several thousand meters, but not in the order of the model size of 30 km or with such a low density due to increasing compaction with depth. Therefore, the impact of density variation on the stress orientation in nature will be much smaller, or on a very local scale. This agrees with the results of Gölke and Coblenz (1996). Observed significant stress rotation are may be a product of other parameters, observation close to the material transition, or low differential stresses.

## 6.3 Stress rotation due to a variation of the Poisson's ratio

390 Model results suggest, that the Variation of the Poisson's ratio can be responsible for a  $S_{Hmax}$  rotation of about  $7.5^\circ$  (Fig. 6). This is below the uncertainties of stress orientation estimations. Therefore, the variation of the Poisson's ratio can be neglected. It was also no literature to detect, investigating that subject.

## 6.4 Stress rotation due to different Young's modulus

The lateral variation of the Young's modulus can lead to significant  $S_{Hmax}$  rotation (Fig. 7). For the used geometry and material  
395 parameters, the relative rotation are up to  $78^\circ$ , which is not far from the maximal possible rotation of  $90^\circ$ . The largest rotation occur in the models with the lower Young's modulus, for example the eee model have a total rotation of  $78^\circ$ , whereas the EEE model provides only  $31^\circ$ . This is not surprising as the Young's modulus is simply a measure of the stiffness. Therefore, largest stress rotation due to stiffness contrast will happen in the soft units not in the rigid ones.

$S_{Hmax}$  will be oriented parallel to the structure for stiff units and perpendicular to weak units, which agrees with the literature  
400 (Bell, 1996b; Zhang et al., 1994). The largest stress rotation occurs nearest to the material transition and decreases with distance to the material transition, similar to other models (Spann et al., 1994). The importance of stiffness differences is an result of other models too (Grünthal and Stromeyer, 1992; Mantovani et al., 2000; Marotta et al., 2002; Spann et al., 1994; Tommasi et al., 1995). In contrast to that, Jarosiński et al. (2006) found, that a stiffness contrast has only minor effects. But they did not test the stiffness contrast separately; they applied that only in combination with active faults in-between the units. However,  
405 this agrees with the results of this study, as faults balance stress rotation by stiffness contrast.

Substantial stress rotations are not observed along major Pre-Mesozoic boundaries and sutures in the eastern United States, like the Greenville front, a suture from Missouri to New York, or in the Appalachian Mountains (Zoback, 1992). Gregersen (1992) reports the same from Fennoscandia. In the case that these tectonic boundaries did not provide a significant stiffness



transition, it is not a contradiction to this study. The observed radial stress pattern southward of the Bohemian massif (Reinecker  
410 and Lenhardt, 1999) agrees well with this study, where  $S_{Hmax}$  is perpendicular in the soft sediments of the Upper and Lower  
Austrian basin directed to the stiff crystalline Bohemian Massif. More ambiguous would that be for the fan shaped pattern in  
western and northern part of the Alpine molasses basin (Grünthal and Stromeyer, 1992; Kastrup et al., 2004; Reinecker et al.,  
2010). As reasons, a lateral stiffness contrast of the rock could play a roll, next to the topographic features of the mountain  
chain and the overall crustal structure.

415 Furthermore, important is the depth of observed stress rotation. For example, data in the north-western Alps are dominant  
focal mechanisms and in the north-eastern Alps the majority of data are from wells, which are more shallow (Reinecker et al.,  
2010).

### 6.5 Comparison of stress rotation due to elastic material properties

The rotation of  $S_{Hmax}$  perpendicular (counter-clockwise) to the structure can be observed in material with a lower Young's  
420 modulus next to a material transition most clearly. Rotation in the same direction, but with a less amount is observed in rocks  
with a larger density or a smaller Poisson's ratio. Within the units having a larger Young's modulus,  $S_{Hmax}$  rotates significant  
parallel (clockwise) to the material transition. Similar rotation with a smaller magnitude can be observed in the low density  
units or in the units with a larger Poisson's ratio. As rocks with a larger Young's modulus will usually have a larger density and  
vice versa (Fig. 3), real rocks will have less  $S_{Hmax}$  rotation as suggested by this generic models.

### 425 6.6 Effect of faults on stress orientation

According to the model results, the influence of low friction faults can be neglected concerning the orientation of the far field  
stress pattern for homogeneous units. The low friction faults lead to only  $3^\circ$   $S_{Hmax}$  rotation in a distance of about 12.5 km next  
to the fault zone. This is not in contrast to the strong stress perturbation, observed in the vicinity of faults as one of the three  
principal stresses must be oriented perpendicular to a fault, the two remaining ones are parallel to the discontinuity (Bell et al.,  
430 1992; Bell, 1996b; Jaeger et al., 2007). Observations from outcrops investigations indicates stress perturbation within 2 km  
(Petit and Mattauer, 1995) or less than 1 km to a fault (Rispoli, 1981); larger stress perturbation is to observe at the termination  
of the fault (2-3 km). If  $S_{Hmax}$  is parallel next to the fault, it will rotate by  $90^\circ$  at the fault termination (Osokina, 1988; Rispoli,  
1981).

Yale (2003) suggests significant stress rotation as a product of active faults within a distance of several hundred meters  
435 for large differential stress provinces and several kilometres for regions with small differential stresses. This is supported by  
observed stress rotations near a fault within a range of a few hundred meters to a few kilometres (Brudy et al., 1997; Yassir  
and Zerwer, 1997). However, not all observed stress rotation agrees to the presented models, like observations offshore eastern  
Canada (Adams and Bell, 1991; Bell and McCallum, 1990) where stress rotation occur in a distance of about 10-15 km to a  
fault.

440 Numerical models investigating stress rotations near a fault provides stress rotation between  $20^\circ$  and  $60^\circ$ , next to the fault,  
depending on the fault strike, the boundary conditions and the friction or weakness of the fault. Near the termination of the



445 fault, stress rotation increases to 50-90° (Homberg et al., 1997; Tommasi et al., 1995; Zhang et al., 1994). However, rotation is observed within 2-3 elements away from the discontinuity, which are anyway needed to distribute the deformation in such numerical models. To avoid this, the orientations of  $S_{Hmax}$  in this study is displayed at least four elements away from the contact surface. In addition, FEM models are unsuitable for representing complex stress-strain patterns near the fault termination if no sufficiently high resolution mesh is available.

## 6.7 Effect of faults combined with stiffness contrasts on stress orientation

450 The models with low friction faults and a variable stiffness (Fig. 9) illustrate much lower stress rotation than the models without the faults (Fig. 7). It seems to be that discontinuities play an important role to reduce stress rotation produced by lateral Young's modulus variation. Regarding to the used model geometry and materials, the  $S_{Hmax}$  variation is reduced for the soft models from 78° to 32°, for eee and lelelel in Figs. 7 and 9, using a friction coefficient of  $\mu = 0.1$ . Also for the mixed models, a change from 78° to 19° is significant. Much lower is the rotation for the stiffer model, with a reduction from 31° to 8° rotation (EEE to lElElEl).

455 The interaction of a variable Young's modulus and presence of low friction faults is visible in Fig. 10. The observed stress rotation strongly depends on the depth. In the soft units,  $S_{Hmax}$  rotates counter-clockwise near the surface (0 to -8 km). In contrast to that a clockwise rotation can be observed in greater depth (18–30 km).

460 The likelihood of seismicity or faults near the interface between stiff and soft units is larger, since differential stresses are greatest there. This fits with the observation of concentrated intraplate earthquakes around cratons (Mooney et al., 2012). On a smaller scale this has been observed for stiff sedimentary layers or rigid dykes, which attracts the occurrence of seismicity (Roberts and Schweitzer, 1999; Ziegler et al., 2015).

## 6.8 Comparison of model results with observed stress orientations

### 6.8.1 Variscan basement in Germany

465 Comparison of modelling results with the stress orientation in the German Variscides is only possible to a certain limit, as the model did not reproduce the detailed structural features of the basement structures and certainly not the (partly) overlying sediments. The comparison will concern only the results of the models investigating the Young's modulus, as this material parameter have the strongest impact. Taking the structural zonation of the European Variscides of Kossmat (1927) into account, cumulative allocation of geomechanical properties is needed to compare the model results. The Rheno-Hercynian Zone (RHZ) and the Northern Phyllite Zone (NPZ) are dominated by clastic shelf sediments with an low- or mid-metamorphic overprint, which are slate (RHZ) and phyllite (NPZ). This zone, the RHZ and the NPZ together, is the weakest, and will have the 470 lowest Young's modulus. The Mid-German Crystalline High (MGCH) consists of granitoids or gabbros and their metamorphic equivalents (gneiss, amphibolite), meta-sediments and some volcanites. Therefore, this zone is a stiff unit. The Saxo-Thuringian Zone (STZ) is dominated by meta-sediments, mafic and felsic magmatites and their metamorphosed equivalents, and some high-grade metamorphic rocks (granulite, eklogite). Taking all the different rock types into account, the STZ is more stiff as

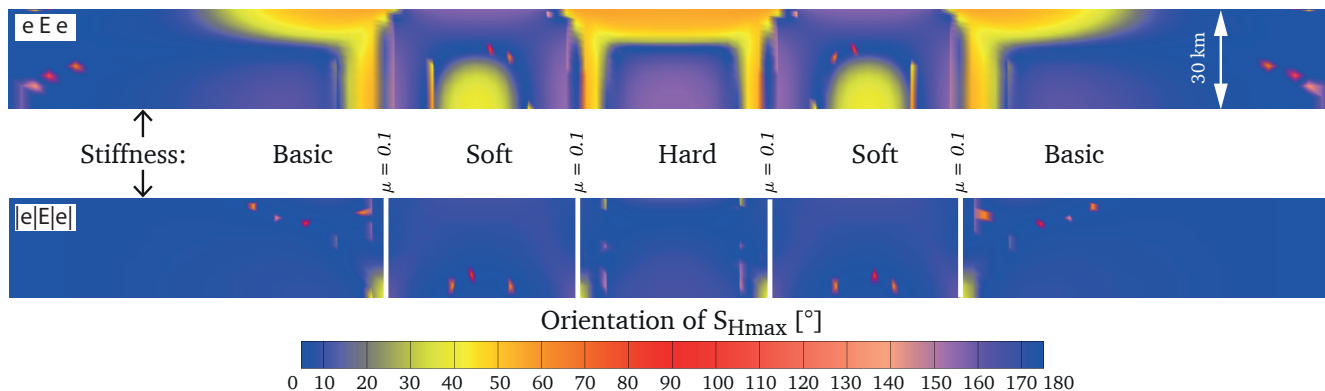


**Figure 10.** North-south depth profiles displaying the  $S_{Hmax}$  orientation colour-coded for a models with variable Young’s modulus. In the model without the discontinuities (eEe),  $S_{Hmax}$  is oriented around  $40^\circ$  in the stiffer units next to the softer units near the Earth surface. A similar orientation can be observed in the soft units in the deepest parts. In contrast to that, in the model with the same material properties, but low friction faults (|e|E|e|), the  $S_{Hmax}$  orientation is nearly north-south for all units and depths. (Small coloured dots are artefacts.) The discontinuities with a low friction coefficient counterbalances stress rotations by stiffness contrasts.

the RHZ and weaker than the MGCH. Mechanical, the Moldanubian zone (MZ) can be represented by high-grade metamorphic  
 475 rocks (gneiss, granulite, migmatite) and granitoids and will be a stiff unit, similar to the MGCH. Therefore, the units are from  
 the deformable to the rigid ones: RHZ < STZ < MGCH  $\approx$  MZ. According to the model results (Fig. 7), the  $S_{Hmax}$  orientation  
 in the RHZ should deflected counter-clockwise, in the STZ slightly counter-clockwise, and clockwise rotation in the MGCH  
 and MZ.

**Table 2.** Material properties used for the Variscan basement units. The properties are estimated based on Turcotte et al. (2002).

Vasiscan units	Density $\rho$ [ $g\ cm^{-3}$ ]	Young’s modulus $E$ [MPa]	Poisson’s ratio $\nu$ [ ]
Rheno-Hercynian (RHZ)	2.10	20	0.15
N. Phillyite (NPZ)	2.20	30	0.15
Mid-German C. (MGCH)	2.75	70	0.30
Saxo-Thuringian (STZ)	2.60	50	0.25
Moldanubian (MZ)	2.75	70	0.30

To do this, adoption of the model with dimensionally appropriate elastic material properties would be the best option. These  
 480 material properties are estimated based on typical rock values (Tab. 2 Turcotte et al., 2002). The same initial stress procedure



and the same boundary condition and visualization as well is applied. The resulting  $S_{Hmax}$  orientation is visualized in Fig. 11 and will be compared with observed  $S_{Hmax}$  orientation in Fig. 1.

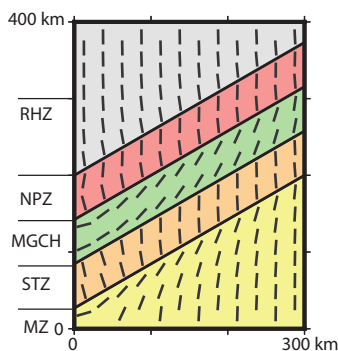


**Figure 11.** Application of estimated material properties of the Variscan units (Tab. 2). Black bars represents the orientations of the maximum horizontal stress ( $S_{Hmax}$ ) at a depth of 1000 m. The equivalent regions are the RHZ = Rheno-Hercynian Zone, NPZ = Northern Phillyite Zone, the MGCH = Mid-German Crystalline High, the STZ = Saxo-Thuringian Zone and the MZ = Moldanubian Zone; compare Fig. 1.

At the transition between the NPZ to the MGCH, a significant clockwise rotation of  $S_{Hmax}$  can be observed within the MGCH (Fig. 11). A much lower but similar stress rotation can be seen at the transition from NPZ to MGCH in Fig. 1 along the river  
485 Rhine. Following that line, crossing the border to the STZ displays a counter-clockwise stress rotation, which is also suggested by the model (Fig. 11). Counter-clockwise rotation is also visible at the same unit boundary near the Main river. In general, the stress orientation in the STZ is counter-clockwise rotated to the orientations from the MGCH unit.  $S_{Hmax}$  orientation from the Harz (Fig. 1) seems to fit quite well to the model results (Fig. 11). However, structures there are complex and other factors could play an important role. Also taking the counter-clockwise rotation of  $S_{Hmax}$  from STZ to the MZ fits with modelling results.  
490 But the stress pattern in the molasses basins is probably more governed by the Alpine orogeny. In general, there are some similarities to observe, but frankly speaking, the model results are not able to prove the significant influence of the material properties on the stress orientation for this region.

Localization of individual grabens and volcanism in the European Cenozoic graben system can be related to late Hercynian fracture systems (Ziegler, 1992). The fan shaped stress pattern in the eastern part of the North German Basin has been explained  
495 as an effect of the close boundary to the stiff Eastern European Craton along the north-west to south-east striking Teisseyre-Tornquist Zone (TTZ, Goes et al., 2000; Gölke and Coblenz, 1996; Grünthal and Stromeyer, 1986, 1992, 1994; Kaiser et al., 2005; Marotta et al., 2002). This agrees well with the results of the models, where  $S_{Hmax}$  becomes perpendicular in a soft unit (NGB) directed to a stiff region like the East European Craton (e.g. model eee in Fig. 7).

Large spatial stress rotations are observed in Australia (Heidbach et al., 2018) and Northern America (Lund Snee and Zoback,  
500 2018, 2020; Reiter et al., 2014). The variable basement structures there and consequently variable mechanical properties are good candidates to explain the complex stress pattern.



## 7 Conclusions

The impact of elastic material parameters (Young's modulus and Poisson's ratio), the body force (density) and low frictions discontinuities on the map view stress pattern is investigated. Each property is tested separately to avoid interdependencies. This is realized with generic 3-D models using the finite element method. Within the models, three units with variable material properties are incorporated, where the boundary conditions govern the overall  $S_{Hmax}$  orientation. The variation of density and the Poisson's ratio lead to small rotation ( $\leq 17^\circ$ ) of the maximum horizontal stress ( $S_{Hmax}$ ). In contrast to that, a stiffness contrast is able to produce significant stress rotation of  $31^\circ$  to  $78^\circ$ . Therefore, the variation of the Young's modulus in the upper crust are a potent explanation for observed stress rotation. Faults are represented in the models by cohesionless contact surfaces. Observed far field stress rotation due to low friction faults ( $\mu = 0.1$ ) is less as  $3^\circ$ . Implementation of low friction discontinuities in models with the Young's modulus anomaly leads to much smaller  $S_{Hmax}$  rotation, in the order of  $8^\circ$  to  $32^\circ$ . Following that, faults did not produce far field stress rotation, they rather compensate stress rotation which are effect by Young's modulus anomaly. Comparison of model results with observed stress orientation in the region, which inspired the models, provides limited consistency.

*Acknowledgements.* Maps and model illustrations were generated using GMT software (Wessel et al., 2013). The author declare that he has no conflict of interest.



## References

- Adams, J. and Bell, J. S.: Crustal Stresses in Canada, in: *Neotectonics of North America*, chap. 20, pp. 367–386, Geological Society of America, 1991.
- 520 Ahorner, L.: Present-day stress field and seismotectonic block movements along major fault zones in Central Europe, *Tectonophysics*, 29, 233–249, [https://doi.org/10.1016/0040-1951\(75\)90148-1](https://doi.org/10.1016/0040-1951(75)90148-1), 1975.
- Amadei, B. and Stephansson, O.: *Rock Stress and Its Measurement*, Chapman & Hall, London, 1997.
- Anderson, E. M.: The dynamics of faulting, *Transactions of the Edinburgh Geological Society*, 8, 387–402, <https://doi.org/10.1144/transed.8.3.387>, 1905.
- 525 Anderson, E. M.: *The Dynamics of Faulting and Dyke Formation with Application to Britain*, 2nd ed. Oliver and Boyd, London and Edinburgh, 1951.
- Artyushkov, E. V.: Stresses in the lithosphere caused by crustal thickness inhomogeneities, *Journal of Geophysical Research*, 78, 7675–7708, <https://doi.org/10.1029/JB078i032p07675>, 1973.
- Assameur, D. M. and Mareschal, J.-C.: Stress induced by topography and crustal density heterogeneities: implication for the seismicity of  
530 southeastern Canada, *Tectonophysics*, 241, 179–192, [https://doi.org/10.1016/0040-1951\(94\)00202-K](https://doi.org/10.1016/0040-1951(94)00202-K), 1995.
- Bada, G., Cloetingh, S., Gerner, P., and Horv ath, F.: Sources of recent tectonic stress in the Pannonian region: inferences from finite element modelling, *Geophysical Journal International*, 134, 87–101, <https://doi.org/10.1046/j.1365-246x.1998.00545.x>, 1998.
- Becker, T. W. and Faccenna, C.: Mantle conveyor beneath the Tethyan collisional belt, *Earth and Planetary Science Letters*, 310, 453–461, <https://doi.org/10.1016/j.epsl.2011.08.021>, 2011.
- 535 Bell, J. S.: In situ stresses in sedimentary rocks (part 1): Measurement techniques, *Geoscience Canada*, 23, 85–100, 1996a.
- Bell, J. S.: In situ stresses in sedimentary rocks (part 2): Applications of stress measurements, *Geoscience Canada*, 23, 135–153, 1996b.
- Bell, J. S. and Gough, D. I.: Northeast-southwest compressive stress in Alberta evidence from oil wells, *Earth and Planetary Science Letters*, 45, 475–482, [https://doi.org/10.1016/0012-821X\(79\)90146-8](https://doi.org/10.1016/0012-821X(79)90146-8), 1979.
- Bell, J. S. and Lloyd, P. F.: Modelling of stress refraction in sediments around the Peace River Arch, Western Canada., *Current Research*,  
540 Part D. Geological Survey of Canada, 89, 49–54, 1989.
- Bell, J. S. and McCallum, R.: In situ stress in the Peace River Arch area, Western Canada, *Bulletin of Canadian Petroleum Geology*, 38, 270–281, 1990.
- Bell, J. S., Caillet, G., and Adams, J.: Attempts to detect open fractures and non-sealing faults with dipmeter logs, *Geological Society, London, Special Publications*, 65, 211–220, <https://doi.org/10.1144/GSL.SP.1992.065.01.16>, 1992.
- 545 Bott, M. H. P. and Dean, D. S.: Stress Systems at Young Continental Margins, *Nature Physical Science*, 235, 23–25, <https://doi.org/10.1038/physci235023a0>, 1972.
- Bott, M. H. P. and Kusznir, N.: Stress distributions associated with compensated plateau uplift structures with application to the continental splitting mechanism, *Geophysical Journal International*, 56, 451–459, <https://doi.org/10.1111/j.1365-246X.1979.tb00177.x>, 1979.
- Bott, M. H. P. and Kusznir, N.: The origin of tectonic stress in the lithosphere, *Tectonophysics*, 105, 1–13, [https://doi.org/10.1016/0040-1951\(84\)90190-2](https://doi.org/10.1016/0040-1951(84)90190-2), 1984.
- 550 Brudy, M., Zoback, M. D., Fuchs, K., Rummel, F., and Baumg artner, J.: Estimation of the complete stress tensor to 8 km depth in the KTB scientific drill holes: Implications for crustal strength, *Journal of Geophysical Research: Solid Earth*, 102, 18453–18475, <https://doi.org/10.1029/96jb02942>, 1997.



- Buchmann, T. J. and Connolly, P. T.: Contemporary kinematics of the Upper Rhine Graben: A 3D finite element approach, *Global and Planetary Change*, 58, 287–309, <https://doi.org/10.1016/j.gloplacha.2007.02.012>, 2007.
- Byerlee, J.: Friction of Rocks, *Pure and Applied Geophysics PAGEOPH*, 116, 615–626, <https://doi.org/10.1007/BF00876528>, 1978.
- Carafa, M. M. C. and Barba, S.: The stress field in Europe: Optimal orientations with confidence limits, *Geophysical Journal International*, 193, 531–548, <https://doi.org/10.1093/gji/ggt024>, 2013.
- Carlsson, A. and Olsson, T.: High rock stresses as a consequence of glaciation, *Nature*, 298, 739–742, <https://doi.org/10.1038/298739a0>, 1982.
- Célérier, B.: Remarks on the relationship between the tectonic regime, the rake of the slip vectors, the dip of the nodal planes, and the plunges of the P, B, and T axes of earthquake focal mechanisms, *Tectonophysics*, 482, 42–49, <https://doi.org/10.1016/j.tecto.2009.03.006>, 2010.
- Chapple, W. M. and Tullis, T. E.: Evaluation of the forces that drive the plates, *Journal of Geophysical Research*, 82, 1967–1984, <https://doi.org/10.1029/JB082i014p01967>, 1977.
- Coblentz, D. D. and Richardson, R. M.: Statistical trends in the intraplate stress field, *Journal of Geophysical Research*, 100, 20 245, <https://doi.org/10.1029/95JB02160>, 1995.
- Cornet, F. H. and Röckel, T.: Vertical stress profiles and the significance of “stress decoupling”, *Tectonophysics*, 581, 193–205, <https://doi.org/10.1016/j.tecto.2012.01.020>, 2012.
- Di Toro, G., Han, R., Hirose, T., De Paola, N., Nielsen, S., Mizoguchi, K., Ferri, F., Cocco, M., and Shimamoto, T.: Fault lubrication during earthquakes, *Nature*, 471, 494–498, <https://doi.org/10.1038/nature09838>, 2011.
- Eisbacher, G. H. and Bielenstein, H. U.: Elastic strain recovery in Proterozoic rocks near Elliot Lake, Ontario, *Journal of Geophysical Research*, 76, 2012–2021, <https://doi.org/10.1029/JB076i008p02012>, 1971.
- Elsasser, W. M.: Sea-floor spreading as thermal convection, *J. Geophys. Res.*, 76, 1101–1112, <https://doi.org/10.1029/JB076i005p01101>, 1971.
- Evans, K. F., Engelder, T., and Plumb, R. A.: Appalachian Stress Study: 1. A detailed description of in situ stress variations in Devonian shales of the Appalachian Plateau, *Journal of Geophysical Research*, 94, 7129, <https://doi.org/10.1029/JB094iB06p07129>, 1989.
- Fleitout, L. and Froidevaux, C.: Tectonics and topography for a lithosphere containing density heterogeneities, *Tectonics*, 1, 21–56, <https://doi.org/10.1029/TC001i001p00021>, 1982.
- Fordjor, C. K., Bell, J. S., and Gough, D. I.: Breakouts in Alberta and stress in the North American plate, *Canadian Journal of Earth Sciences*, 20, 1445–1455, <https://doi.org/10.1139/e83-130>, 1983.
- Forsyth, D. W. and Uyeda, S.: On the Relative Importance of the Driving Forces of Plate Motion, *Geophysical Journal International*, 43, 163–200, <https://doi.org/10.1111/j.1365-246X.1975.tb00631.x>, 1975.
- Frank, F. C.: Plate Tectonics, the Analogy with Glacier Flow, and Isostasy, in: *Flow and Fracture of Rocks*, edited by Heard, H. C., Borg, I. Y., Carter, N. L., and Raleigh, C. B., pp. 285–292, AGU, Washington D.C., geophysica edn., <https://doi.org/10.1029/GM016p0285>, 1972.
- Franke, W.: The mid-European segment of the Variscides: tectonostratigraphic units, terrane boundaries and plate tectonic evolution, *Geological Society, London, Special Publications*, 179, 35–61, <https://doi.org/10.1144/GSL.SP.2000.179.01.05>, 2000.
- Franke, W.: The Variscan orogen in Central Europe: construction and collapse, *Geological Society, London, Memoirs*, 32, 333–343, <https://doi.org/10.1144/GSL.MEM.2006.032.01.20>, 2006.
- Franke, W.: Topography of the Variscan orogen in Europe: Failed-not collapsed, *International Journal of Earth Sciences*, 103, 1471–1499, <https://doi.org/10.1007/s00531-014-1014-9>, 2014.



- 595 Franke, W. and Dulce, J.-C.: Back to sender: tectonic accretion and recycling of Baltica-derived Devonian clastic sediments in the Rheno-Hercynian Variscides, *International Journal of Earth Sciences*, 106, 377–386, <https://doi.org/10.1007/s00531-016-1408-y>, 2017.
- Froidevaux, C., Paquin, C., and Souriau, M.: Tectonic stresses in France: In situ measurements with a flat jack, *Journal of Geophysical Research: Solid Earth*, 85, 6342–6346, <https://doi.org/10.1029/JB085iB11p06342>, 1980.
- Ghosh, A., Holt, W. E., Flesch, L. M., and Haines, A. J.: Gravitational potential energy of the Tibetan Plateau and the forces driving the Indian plate, *Geology*, 34, 321–324, <https://doi.org/10.1130/G22071.1>, 2006.
- Ghosh, A., Holt, W. E., and Flesch, L. M.: Contribution of gravitational potential energy differences to the global stress field, *Geophysical Journal International*, 179, 787–812, <https://doi.org/10.1111/j.1365-246X.2009.04326.x>, 2009.
- 600 Ghosh, A., Holt, W. E., and Wen, L.: Predicting the lithospheric stress field and plate motions by joint modeling of lithosphere and mantle dynamics, *Journal of Geophysical Research: Solid Earth*, 118, 346–368, <https://doi.org/10.1029/2012JB009516>, 2013.
- Goes, S., Loohuis, J., Wortel, M., and Govers, R.: The effect of plate stresses and shallow mantle temperatures on tectonics of northwestern Europe, *Global and Planetary Change*, 27, 23–38, [https://doi.org/10.1016/S0921-8181\(01\)00057-1](https://doi.org/10.1016/S0921-8181(01)00057-1), 2000.
- Gölke, M. and Coblenz, D. D.: Origins of the European regional stress field, *Tectonophysics*, 266, 11–24, [https://doi.org/10.1016/S0040-1951\(96\)00180-1](https://doi.org/10.1016/S0040-1951(96)00180-1), 1996.
- 605 Gough, D. I.: Mantle upflow under North America and plate dynamics, *Nature*, 311, 428–433, <https://doi.org/10.1038/311428a0>, 1984.
- Grad, M. and Tiira, T.: The Moho depth map of the European Plate, *Geophysical Journal International*, 176, 279–292, <https://doi.org/10.1111/j.1365-246X.2008.03919.x>, 2009.
- Grad, M., Polkowski, M., and Ostaficzuk, S. R.: High-resolution 3D seismic model of the crustal and uppermost mantle structure in Poland, *Tectonophysics*, 666, 188–210, <https://doi.org/10.1016/j.tecto.2015.10.022>, 2016.
- 610 Gregersen, S.: Crustal stress regime in Fennoscandia from focal mechanisms, *Journal of Geophysical Research*, 97, 11 821, <https://doi.org/10.1029/91JB02011>, 1992.
- Greiner, G.: In-situ stress measurements in Southwest Germany, *Tectonophysics*, 29, 265–274, [https://doi.org/10.1016/0040-1951\(75\)90150-X](https://doi.org/10.1016/0040-1951(75)90150-X), 1975.
- 615 Greiner, G. and Illies, J. H.: Central Europe: Active or residual tectonic stresses, *Pure and Applied Geophysics PAGEOPH*, 115, 11–26, <https://doi.org/10.1007/BF01637094>, 1977.
- Grünthal, G. and Stromeyer, D.: Stress pattern in Central Europe and adjacent areas, *Gerlands Beitr. Geophysik*, 95, 443–452, 1986.
- Grünthal, G. and Stromeyer, D.: The recent crustal stress field in central Europe: Trajectories and finite element modeling, *Journal of Geophysical Research*, 97, 11 805–11 820, <https://doi.org/10.1029/91JB01963>, 1992.
- 620 Grünthal, G. and Stromeyer, D.: The recent crustal stress field in central Europe sensu lato and its quantitative modelling, *Geologie en Mijnbouw*, 73, 173–180, 1994.
- Hast, N.: The state of stress in the upper part of the earth's crust, *Tectonophysics*, 8, 169–211, [https://doi.org/10.1016/0040-1951\(69\)90097-3](https://doi.org/10.1016/0040-1951(69)90097-3), 1969.
- Hast, N.: Global Measurements of Absolute Stress, *Philosophical Transactions of the Royal Society A: Mathematical, Physical and Engineering Sciences*, 274, 409–419, <https://doi.org/10.1098/rsta.1973.0070>, 1973.
- 625 Hast, N.: The state of stress in the upper part of the Earth's crust as determined by measurements of absolute rock stress, *Die Naturwissenschaften*, 61, 468–475, <https://doi.org/10.1007/BF00622962>, 1974.
- Haxby, W. F. and Turcotte, D. L.: Stresses induced by the addition or removal of overburden and associated thermal effects, *Geology*, 4, 21–56, [https://doi.org/10.1130/0091-7613\(1976\)4<181:SIBTAO>2.0.CO;2](https://doi.org/10.1130/0091-7613(1976)4<181:SIBTAO>2.0.CO;2), 1976.



- 630 Heidbach, O., Reinecker, J., Tingay, M. R. P., Müller, B., Sperner, B., Fuchs, K., and Wenzel, F.: Plate boundary forces are not enough: Second- and third-order stress patterns highlighted in the World Stress Map database, *Tectonics*, 26, 1–19, <https://doi.org/10.1029/2007TC002133>, 2007.
- Heidbach, O., Tingay, M. R. P., Barth, A., Reinecker, J., Kurfeß, D., and Müller, B.: Global crustal stress pattern based on the World Stress Map database release 2008, *Tectonophysics*, 482, 3–15, <https://doi.org/10.1016/j.tecto.2009.07.023>, 2010.
- 635 Heidbach, O., Rajabi, M., Cui, X., Fuchs, K., Müller, B., Reinecker, J., Reiter, K., Tingay, M. R. P., Wenzel, F., Xie, F., Ziegler, M. O., Zoback, M.-L., and Zoback, M. D.: The World Stress Map database release 2016: Crustal stress pattern across scales, *Tectonophysics*, 744, 484–498, <https://doi.org/10.1016/j.tecto.2018.07.007>, 2018.
- Hergert, T. and Heidbach, O.: Geomechanical model of the Marmara Sea region-II. 3-D contemporary background stress field, *Geophysical Journal International*, 185, 1090–1102, <https://doi.org/10.1111/j.1365-246X.2011.04992.x>, 2011.
- 640 Hergert, T., Heidbach, O., Reiter, K., Giger, S. B., and Marschall, P.: Stress field sensitivity analysis in a sedimentary sequence of the Alpine foreland, northern Switzerland, *Solid Earth*, 6, 533–552, <https://doi.org/10.5194/se-6-533-2015>, 2015.
- Herget, G.: Variation of rock stresses with depth at a Canadian iron mine, *International Journal of Rock Mechanics and Mining Sciences & Geomechanics Abstracts*, 10, 37–51, [https://doi.org/10.1016/0148-9062\(73\)90058-2](https://doi.org/10.1016/0148-9062(73)90058-2), 1973.
- Hickman, S. H. and Zoback, M. D.: Stress orientations and magnitudes in the SAFOD pilot hole, *Geophysical Research Letters*, 31, L15S12, <https://doi.org/10.1029/2004GL020043>, 2004.
- 645 Homberg, C., Hu, J., Angelier, J., Bergerat, F., and Lacombe, O.: Characterization of stress perturbations near major fault zones: insights from 2-D distinct-element numerical modelling and field studies (Jura mountains), *Journal of Structural Geology*, 19, 703–718, 1997.
- Hottman, C., Smith, J., and Purcell, W.: Relationship Among Earth Stresses, Pore Pressure, and Drilling Problems Offshore Gulf of Alaska, *Journal of Petroleum Technology*, 31, 1477–1484, <https://doi.org/10.2118/7501-PA>, 1979.
- 650 Humphreys, E. D. and Coblenz, D. D.: North American dynamics and western U.S. tectonics, *Reviews of Geophysics*, 45, <https://doi.org/10.1029/2005RG000181>, 2007.
- Jaeger, J. C., Cook, N., and Zimmerman, R.: *Fundamentals of rock mechanics*, Blackwell, 4th edn., 2007.
- Jarosiński, M., Beekman, F., Bada, G., Cloetingh, S., and Jarosinski, M.: Redistribution of recent collision push and ridge push in Central Europe: insights from FEM modelling, *Geophysical Journal International*, 167, 860–880, <https://doi.org/10.1111/j.1365-246X.2006.02979.x>, 2006.
- 655 Kaiser, A., Reicherter, K., Hübscher, C., and Gajewski, D.: Variation of the present-day stress field within the North German Basin - Insights from thin shell FE modeling based on residual GPS velocities, *Tectonophysics*, 397, 55–72, <https://doi.org/10.1016/j.tecto.2004.10.009>, 2005.
- Kastrup, U., Zoback, M.-L. L., Deichmann, N., Evans, K. F., Giardini, D., and Michael, A. J.: Stress field variations in the Swiss Alps and the northern Alpine foreland derived from inversion of fault plane solutions, *Journal of Geophysical Research: Solid Earth*, 109, B01402, <https://doi.org/10.1029/2003jb002550>, 2004.
- 660 King, R., Backé, G., Tingay, M., Hillis, R., and Mildren, S.: Stress deflections around salt diapirs in the Gulf of Mexico, *Geological Society, London, Special Publications*, 367, 141–153, <https://doi.org/10.1144/SP367.10>, 2012.
- Klein, R. and Barr, M.: Regional state of stress in western Europe, in: *Rock stress and rock stress measurement*, pp. 33–44, *International Society for Rock Mechanics and Rock Engineering*, Stockholm, 1986.
- 665 Klügel, T., Ahrendt, H., Oncken, O., Käfer, N., Schäfer, F., and Weiss, B.: Alter und Herkunft der Sedimente und des Detritus der nördlichen Phyllit-Zone (Taunussüdrand), *Zeitschrift der Deutschen Geologischen Gesellschaft*, pp. 172–191, 1994.



- Kohlbeck, F., Roch, K.-H., and Scheidegger, A. E.: In Situ Stress Measurements in Austria, in: Tectonic Stresses in the Alpine-Mediterranean Region, edited by Scheidegger, A. E., pp. 21–29, Springer Vienna, Vienna, [https://doi.org/10.1007/978-3-7091-8588-9\\_5](https://doi.org/10.1007/978-3-7091-8588-9_5), 1980.
- 670 Kossmat, F.: Gliederung des varistischen Gebirgsbaues, *Abhandlungen des Sächsischen Geologischen Landesamtes*, 1, 1–39, 1927.
- Kroner, U. and Romer, R. L.: Two plates - Many subduction zones: The Variscan orogeny reconsidered, *Gondwana Research*, 24, 298–329, <https://doi.org/10.1016/j.gr.2013.03.001>, 2013.
- Kroner, U., Hahn, T., Romer, R. L., and Linnemann, U.: The Variscan orogeny in the Saxo-Thuringian zone—heterogenous overprint of Cadomian/Paleozoic peri-Gondwana crust, Special Paper 423: The Evolution of the Rheic Ocean: From Avalonian-Cadomian Active Margin to Alleghenian-Variscan Collision, 423, 153–172, [https://doi.org/10.1130/2007.2423\(06\)](https://doi.org/10.1130/2007.2423(06)), 2007.
- 675 Laubach, S. E., Clift, S. J., Hill, R. E., and Fix, J.: Stress Directions in Cretaceous Frontier Formation, Green River Basin, Wyoming, in: *Rediscover the Rockies; 43rd Annual Field Conference Guidebook*, pp. 75–86, 1992.
- Linnemann, U. e.: *Das Saxothuringikum: Abriss der präkambrischen und paläozoischen Geologie von Sachsen und Thüringen*, Staatliche Naturhistorische Sammlung Dresden, Museum für Mineralogie und Geologie, Dresden, geologican edn., 2004.
- 680 Lithgow-Bertelloni, C.: Origin of the lithospheric stress field, *Journal of Geophysical Research*, 109, 1–32, <https://doi.org/10.1029/2003JB002467>, 2004.
- Lund, B. and Zoback, M. D.: Orientation and magnitude of in situ stress to 6.5 km depth in the Baltic Shield, *International Journal of Rock Mechanics and Mining Sciences*, 36, 169–190, [https://doi.org/10.1016/S0148-9062\(98\)00183-1](https://doi.org/10.1016/S0148-9062(98)00183-1), 1999.
- Lund Snee, J.-E. and Zoback, M. D.: State of stress in the Permian Basin, Texas and New Mexico: Implications for induced seismicity, *The Leading Edge*, 37, 127–134, <https://doi.org/10.1190/tle37020127.1>, 2018.
- 685 Lund Snee, J.-E. and Zoback, M. D.: Multiscale variations of the crustal stress field throughout North America, *Nature Communications*, pp. 1–9, <https://doi.org/10.1038/s41467-020-15841-5>, 2020.
- Mantovani, E., Viti, M., Albarello, D., Tamburelli, C., Babbucci, D., and Cenni, N.: Role of kinematically induced horizontal forces in Mediterranean tectonics: insights from numerical modeling, *Journal of Geodynamics*, 30, 287–320, [https://doi.org/10.1016/S0264-3707\(99\)00067-8](https://doi.org/10.1016/S0264-3707(99)00067-8), 2000.
- 690 Marotta, A. M., Bayer, U., Thybo, H., and Scheck-Wenderoth, M.: Origin of the regional stress in the North German basin: Results from numerical modelling, *Tectonophysics*, 360, 245–264, [https://doi.org/10.1016/S0040-1951\(02\)00358-X](https://doi.org/10.1016/S0040-1951(02)00358-X), 2002.
- Martínez-Garzón, P., Bohnhoff, M., Kwiatek, G., and Dresen, G.: Stress tensor changes related to fluid injection at The Geysers geothermal field, California, *Geophysical Research Letters*, 40, 2596–2601, <https://doi.org/10.1002/grl.50438>, 2013.
- 695 Matte, P.: Tectonics and plate tectonics model for the Variscan belt of Europe, *Tectonophysics*, 126, [https://doi.org/10.1016/0040-1951\(86\)90237-4](https://doi.org/10.1016/0040-1951(86)90237-4), 1986.
- Mazzotti, S. and Townend, J.: State of stress in central and eastern North American seismic zones, *Lithosphere*, 2, 76–83, <https://doi.org/10.1130/l65.1>, 2010.
- McGarr, A.: Analysis of states of stress between provinces of constant stress, *Journal of Geophysical Research*, 87, 9279, <https://doi.org/10.1029/JB087iB11p09279>, 1982.
- 700 McGarr, A. and Gay, N. C.: State of stress in the earth's crust, *Annual Review of Earth and Planetary Sciences*, 6, 405–436, [https://doi.org/10.1016/0040-1951\(64\)90010-1](https://doi.org/10.1016/0040-1951(64)90010-1), 1978.
- Miller, D. J. and Dunne, T.: Topographic perturbations of regional stresses and consequent bedrock fracturing, *Journal of Geophysical Research: Solid Earth*, 101, 25 523–25 536, <https://doi.org/10.1029/96JB02531>, 1996.



- 705 Minster, J. B. and Jordan, T. H.: Present-day plate motions, *Journal of Geophysical Research*, 83, 5331, <https://doi.org/10.1029/JB083iB11p05331>, 1978.
- Mooney, W. D., Ritsema, J., and Hwang, Y. K.: Crustal seismicity and the earthquake catalog maximum moment magnitude ( $M_{\max}$ ) in stable continental regions (SCRs): Correlation with the seismic velocity of the lithosphere, *Earth and Planetary Science Letters*, 357–358, 78–83, <https://doi.org/10.1016/j.epsl.2012.08.032>, 2012.
- 710 Müller, B., Zoback, M.-L., Fuchs, K., Mastin, L., Gregersen, S., Pavoni, N., Stephansson, O., and Ljunggren, C.: Regional patterns of tectonic stress in Europe, *Journal of Geophysical Research*, 97, 11 783, <https://doi.org/10.1029/91JB01096>, 1992.
- Müller, B., Wehrle, V., Zeyen, H., and Fuchs, K.: Short-scale variations of tectonic regimes in the western European stress province north of the Alps and Pyrenees, *Tectonophysics*, 275, 199–219, [https://doi.org/10.1016/S0040-1951\(97\)00021-8](https://doi.org/10.1016/S0040-1951(97)00021-8), 1997.
- Müller, B., Heidbach, O., Negut, M., Sperner, B., and Buchmann, T. J.: Tectonophysics Attached or not attached — evi-  
715 dence from crustal stress observations for a weak coupling of the Vrancea slab in Romania, *Tectonophysics*, 482, 139–149, <https://doi.org/10.1016/j.tecto.2009.08.022>, 2010.
- Müller, B., Schilling, F., Röckel, T., and Heidbach, O.: Induced Seismicity in Reservoirs : Stress Makes the Difference, *Erdöl Erdgas Kohle*, 134, 33–37, <https://doi.org/10.19225/180106>, 2018.
- Müller, S. and Zürich, E. T. H.: Tiefenstruktur, Dynamik und Entwicklung des Mittelmeer- und Alpenraumes, *Vierteljahrsschrift der Natur-  
720 forschenden Gesellschaft in Zürich*, 129, 217–245, 1984.
- Naliboff, J. B., Lithgow-Bertelloni, C., Ruff, L. J., and de Koker, N.: The effects of lithospheric thickness and density structure on Earth's stress field, *Geophysical Journal International*, 188, 1–17, <https://doi.org/10.1111/j.1365-246X.2011.05248.x>, 2012.
- Oncken, O.: Transformation of a magmatic arc and an orogenic root during oblique collision and its consequences for the evolution of the European Variscides (Mid-German Crystalline Rise), *Geologische Rundschau*, 86, 2–20, <https://doi.org/10.1007/s005310050118>, 1997.
- 725 Oncken, O., Franzke, H. J., Dittmar, U., and Klügel, T.: Rhenohercynian foldbelt: Metamorphic Units (Northern Phyllite Zone), *Structure*, in: *Pre-Permian Geology of Central and Western Europe*, edited by Dallmeyer, R. D., Franke, W., and Weber, K., pp. 109–117, Springer, Berlin, 1995.
- Osokina, D.: Hierarchical properties of a stress field and its relation to fault displacements, *Journal of Geodynamics*, 10, 331–344, [https://doi.org/10.1016/0264-3707\(88\)90039-7](https://doi.org/10.1016/0264-3707(88)90039-7), 1988.
- 730 Petit, J. P. and Mattauer, M.: Palaeostress superimposition deduced from mesoscale structures in limestone: the Matelles exposure, Languedoc, France, *Journal of Structural Geology*, 17, 245–256, [https://doi.org/10.1016/0191-8141\(94\)E0039-2](https://doi.org/10.1016/0191-8141(94)E0039-2), 1995.
- Pierdominici, S. and Heidbach, O.: Stress field of Italy — Mean stress orientation at different depths and wave-length of the stress pattern, *Tectonophysics*, 532–535, 301–311, <https://doi.org/10.1016/j.tecto.2012.02.018>, 2012.
- Plumb, R. A. and Cox, J. W.: Stress directions in eastern North America determined to 4.5 km from borehole elongation measurements,  
735 *Journal of Geophysical Research*, 92, 4805, <https://doi.org/10.1029/JB092iB06p04805>, 1987.
- Plumb, R. A. and Hickman, S. H.: Stress-induced borehole elongation: A comparison between the four-arm dipmeter and the borehole televiewer in the Auburn Geothermal Well, *Journal of Geophysical Research*, 90, 5513–5521, <https://doi.org/10.1029/JB090iB07p05513>, 1985.
- Ranalli, G. and Chandler, T. E.: The Stress Field in the Upper Crust as Determined from In Situ Measurements, *Geologische Rundschau*, 64,  
740 653–674, <https://doi.org/10.1007/BF01820688>, 1975.
- Rebaï, S., Philip, H., and Taboada, A.: Modern tectonic stress field in the Mediterranean region: evidence for variation in stress directions at different scales, *Geophysical Journal International*, 110, 106–140, <https://doi.org/10.1111/j.1365-246X.1992.tb00717.x>, 1992.



- Reinecker, J. and Lenhardt, W. A.: Present-day stress field and deformation in eastern Austria, *International Journal of Earth Sciences*, 88, 532–550, <https://doi.org/10.1007/s005310050283>, 1999.
- 745 Reinecker, J., Tingay, M. R. P., Müller, B., and Heidbach, O.: Present-day stress orientation in the Molasse Basin, *Tectonophysics*, 482, 129–138, <https://doi.org/10.1016/j.tecto.2009.07.021>, 2010.
- Reiter, K. and Heidbach, O.: 3-D geomechanical–numerical model of the contemporary crustal stress state in the Alberta Basin (Canada), *Solid Earth*, 5, 1123–1149, <https://doi.org/10.5194/se-5-1123-2014>, 2014.
- Reiter, K., Heidbach, O., Schmitt, D. R., Haug, K., Ziegler, M. O., and Moeck, I. S.: A revised crustal stress orientation database for Canada, *Tectonophysics*, 636, 111–124, <https://doi.org/10.1016/j.tecto.2014.08.006>, 2014.
- 750 Reiter, K., Heidbach, O., Reinecker, J., Müller, B., and Röckel, T.: Spannungskarte Deutschland 2015, *Erdöl Erdgas Kohle*, 131, 437–442, <https://doi.org/10.1029/98EO00426>, 2015.
- Richardson, R. M.: Ridge forces, absolute plate motions, and the intraplate stress field, *Journal of Geophysical Research*, 97, 11 739, <https://doi.org/10.1029/91JB00475>, 1992.
- 755 Richardson, R. M. and Reding, L. M.: North American Plate Dynamics, *Journal of Geophysical Research*, 96, 12 201–12 223, <https://doi.org/10.1029/91JB00958>, 1991.
- Richardson, R. M., Solomon, S. C., and Sleep, N. H.: Intraplate stress as an indicator of plate tectonic driving forces, *Journal of Geophysical Research*, 81, 1847–1856, <https://doi.org/10.1029/JB081i011p01847>, 1976.
- Richardson, R. M., Solomon, S. C., and Sleep, N. H.: Tectonic stress in the plates, *Reviews of Geophysics*, 17, 981–1019, <https://doi.org/10.1029/RG017i005p00981>, 1979.
- 760 Rispoli, R.: Stress fields about strike-slip faults inferred from stylolites and tension gashes, *Tectonophysics*, 75, T29–T36, [https://doi.org/10.1016/0040-1951\(81\)90274-2](https://doi.org/10.1016/0040-1951(81)90274-2), 1981.
- Roberts, M. and Schweitzer, J.: Geotechnical areas associated with the Ventersdorp Contact Reef, Witwatersrand Basin, South Africa, *Journal of the South African Institute of Mining and Metallurgy*, 99, 157–166, 1999.
- 765 Röckel, T. and Lempp, C.: Der Spannungszustand im Norddeutschen Becken, *Erdoel Erdgas Kohle*, 119, 73–80, 2003.
- Roth, F. and Fleckenstein, P.: Stress orientations found in North-East Germany differ from the West European trend, *Terra Nova*, 13, 289–296, <https://doi.org/10.1046/j.1365-3121.2001.00357.x>, 2001.
- Savage, W. Z. and Swolfs, H. S.: Tectonic and gravitational stress in long symmetric ridges and valleys, *Journal of Geophysical Research*, 91, 3677, <https://doi.org/10.1029/JB091iB03p03677>, 1986.
- 770 Sbar, M. L. and Sykes, L. R.: Contemporary Compressive Stress and Seismicity in Eastern North America: An Example of Intra-Plate Tectonics, *Geological Society of America Bulletin*, 84, 1861–1882, [https://doi.org/10.1130/0016-7606\(1973\)84<1861:CCSASI>2.0.CO;2](https://doi.org/10.1130/0016-7606(1973)84<1861:CCSASI>2.0.CO;2), 1973.
- Schmitt, D. R., Currie, C. A., and Zhang, L.: Crustal stress determination from boreholes and rock cores: Fundamental principles, *Tectonophysics*, 580, 1–26, <https://doi.org/10.1016/j.tecto.2012.08.029>, 2012.
- 775 Schoenball, M. and Davatzes, N. C.: Quantifying the heterogeneity of the tectonic stress field using borehole data, *Journal of Geophysical Research: Solid Earth*, 122, 6737–6756, <https://doi.org/10.1002/2017JB014370>, 2017.
- Sonder, L. J.: Effects of density contrasts on the orientation of stresses in the lithosphere: Relation to principal stress directions in the Transverse Ranges, California, *Tectonics*, 9, 761–771, <https://doi.org/10.1029/TC009i004p00761>, 1990.
- Spann, H., Müller, B., and Fuchs, K.: Interpretation of anomalies in observed stress data at the central graben (north sea) - numerical and analytical approach, *Soil Dynamics and Earthquake Engineering*, 13, 1–11, [https://doi.org/10.1016/0267-7261\(94\)90036-1](https://doi.org/10.1016/0267-7261(94)90036-1), 1994.
- 780



- Sperner, B., Müller, B., Heidbach, O., Delvaux, D., Reinecker, J., and Fuchs, K.: Tectonic stress in the Earth's crust: advances in the World Stress Map project, Geological Society Special Publication, 212, 101–116, 2003.
- Stein, S., Cloetingh, S., Sleep, N. H., and Wortel, R.: Passive Margin Earthquakes, Stresses and Rheology, in: Earthquakes at North-Atlantic Passive Margins: Neotectonics and Postglacial Rebound, pp. 231–259, Springer Netherlands, Dordrecht, [https://doi.org/10.1007/978-94-009-2311-9\\_14](https://doi.org/10.1007/978-94-009-2311-9_14), 1989.
- 785 Steinberger, B., Schmelting, H., and Marquart, G.: Large-scale lithospheric stress field and topography induced by global mantle circulation, Earth and Planetary Science Letters, 186, 75–91, 2001.
- Stephansson, O. and Berner, H.: The finite element method in tectonic processes, Physics of the Earth and Planetary Interiors, 4, 301–321, [https://doi.org/10.1016/0031-9201\(71\)90014-8](https://doi.org/10.1016/0031-9201(71)90014-8), 1971.
- 790 Tesauro, M., Kaban, M. K., and Cloetingh, S. A.: Global strength and elastic thickness of the lithosphere, Global and Planetary Change, 90–91, 51–57, <https://doi.org/10.1016/j.gloplacha.2011.12.003>, 2012.
- Tingay, M. R. P., Müller, B. B., Reinecker, J., Heidbach, O., Wenzel, F., and Fleckenstein, P.: Understanding tectonic stress in the oil patch: The World Stress Map Project, The Leading Edge, 24, 1276–1282, <https://doi.org/10.1190/1.2149653>, 2005.
- Tommasi, A., Vauchez, A., and Daudré, B.: Initiation and propagation of shear zones in a heterogeneous continental lithosphere, Journal of Geophysical Research: Solid Earth, 100, 22 083–22 101, <https://doi.org/10.1029/95JB02042>, 1995.
- 795 Tullis, T. E.: Reflections on Measurement of Residual-Stress in Rock, Pure and Applied Geophysics, 115, 57–68, <https://doi.org/10.1007/bf01637097>, 1977.
- Turcotte, D. L.: Are transform faults thermal contraction cracks?, Journal of Geophysical Research, 79, 2573–2577, <https://doi.org/10.1029/JB079i017p02573>, 1974a.
- 800 Turcotte, D. L.: Membrane Tectonics, Geophysical Journal International, 36, 33–42, 1974b.
- Turcotte, D. L. and Oxburgh, E.: Stress accumulation in the lithosphere, Tectonophysics, 35, 183–199, [https://doi.org/10.1016/0040-1951\(76\)90037-8](https://doi.org/10.1016/0040-1951(76)90037-8), 1976.
- Turcotte, D. L. and Oxburgh, E. R.: Mid-plate Tectonics, Nature, 244, 337–339, <https://doi.org/10.1038/244337a0>, 1973.
- Turcotte, D. L., Schubert, and Schubert, G.: Geodynamics, Cambridge University Press, 2002.
- 805 Turner, M., Clough, R., Martin, H., and Topp, L.: Stiffness and Deflection Analysis of Complex Structures, Journal of the Aeronautical Sciences, 23, 805–823, 1956.
- Walcott, R. I.: Flexural rigidity, thickness, and viscosity of the lithosphere, Journal of Geophysical Research, 75, 3941–3954, <https://doi.org/10.1029/JB075i020p03941>, 1970.
- Wessel, P., Smith, W. H. F., Scharroo, R., Luis, J., and Wobbe, F.: Generic mapping tools: Improved version released, Eos, 94, 409–410, <https://doi.org/10.1002/2013EO450001>, 2013.
- 810 Wu, P. and Johnston, P.: Can deglaciation trigger earthquakes in N. America?, Geophysical Research Letters, 27, 1323, <https://doi.org/10.1029/1999GL011070>, 2000.
- Yale, D. P.: Fault and stress magnitude controls on variations in the orientation of in situ stress, Geological Society, London, Special Publications, 209, 55–64, <https://doi.org/10.1144/GSL.SP.2003.209.01.06>, 2003.
- 815 Yassir, N. A. and Zerwer, A.: Stress regimes in the Gulf coast, offshore Louisiana: Data from well-bore breakout analysis, AAPG Bulletin, 81, 293–307, <https://doi.org/10.1306/522B4311-1727-11D7-8645000102C1865D>, 1997.
- Zakharova, N. V. and Goldberg, D. S.: In situ stress analysis in the northern Newark Basin: implications for induced seismicity from CO<sub>2</sub> injection, Journal of Geophysical Research: Solid Earth, 119, 1–13, <https://doi.org/10.1002/2013JB010492>.Received, 2014.



- 820 Zang, A. and Stephansson, O.: Stress Field of the Earth's Crust, Springer Netherlands, Dordrecht, <https://doi.org/10.1007/978-1-4020-8444-7>, 2010.
- Zhang, Y.-Z., Dusseault, M. B., and Yassir, N. A.: Effects of rock anisotropy and heterogeneity on stress distributions at selected sites in North America, *Engineering Geology*, 37, 181–197, [https://doi.org/10.1016/0013-7952\(94\)90055-8](https://doi.org/10.1016/0013-7952(94)90055-8), 1994.
- Ziegler, M., Reiter, K., Heidbach, O., Zang, A., Kwiatek, G., Stromeyer, D., Dahm, T., Dresen, G., Hofmann, G., Stromeyer, D., Dahm, T., Dresen, G., and Hofmann, G.: Mining-Induced Stress Transfer and Its Relation to a  $M_w = 1.9$  Seismic Event in an Ultra-deep South African Gold Mine, *Pure and Applied Geophysics*, 172, 2557–2570, <https://doi.org/10.1007/s00024-015-1033-x>, 2015.
- 825 Ziegler, M. O., Heidbach, O., Zang, A., Martínez-Garzón, P., and Bohnhoff, M.: Estimation of the differential stress from the stress rotation angle in low permeable rock, *Geophysical Research Letters*, 44, 6761–6770, <https://doi.org/10.1002/2017GL073598>, 2017.
- Ziegler, P. A.: European Cenozoic rift system, *Tectonophysics*, 208, 91–111, [https://doi.org/10.1016/0040-1951\(92\)90338-7](https://doi.org/10.1016/0040-1951(92)90338-7), 1992.
- Zoback, M. D. and Zoback, M.-L.: State of Stress and Intraplate Earthquakes in the United States, *Science*, 213, 96–104, <https://doi.org/10.1126/science.213.4503.96>, 1981.
- 830 Zoback, M.-L.: First- and second-order patterns of stress in the lithosphere: The World Stress Map Project, *Journal of Geophysical Research*, 97, 11 703–11 728, <https://doi.org/10.1029/92JB00132>, 1992.
- Zoback, M.-L., Zoback, M. D., Adams, J., Assumpção, M., Bell, J. S., Bergman, E. A., Blümling, P., Brereton, N. R., Denham, D., Ding, J., Fuchs, K., Gay, N., Gregersen, S., Gupta, H. K., Gvishiani, A., Jacob, K., Klein, R., Knoll, P., Magee, M., Mercier, J. L., Müller, B., Paquin, C., Rajendran, K., Stephansson, O., Suarez, G., Suter, M., Udias, A., Xu, Z. H., and Zhizhin, M.: Global patterns of tectonic stress, *Nature*, 341, 291–298, <https://doi.org/10.1038/341291a0>, 1989.
- 835 Zoback, M.-L. L. and Mooney, W. D.: Lithospheric Buoyancy and Continental Intraplate Stresses, *International Geology Review*, 45, 95–118, <https://doi.org/10.2747/0020-6814.45.2.95>, 2003.
- Zoback, M. M. D., Moos, D., Mastin, L., and Anderson, R. N.: Well bore breakouts and in situ stress, *Journal of Geophysical Research*, 90, 840 5523–5530, <https://doi.org/10.1029/JB090iB07p05523>, 1985.